2017

SH3 AND MULTIPLE ANKYRIN REPEAT DOMAIN 3 (SHANK3) AFFECTS THE EXPRESSION OF HYPERPOLARIZATION-ACTIVATED CYCLIC NUCLEOTIDE-GATED (HCN) CHANNELS IN MOUSE MODELS OF AUTISM

Nikhil N. Shah
Virginia Commonwealth University

SH3 AND MULTIPLE ANYKRIN REPEAT DOMAIN 3 (SHANK3) AFFECTS THE EXPRESSION OF HYPERPOLARIZATION-ACTIVATED CYCLIC NUCLEOTIDE-GATED (HCN) CHANNELS IN MOUSE MODELS OF AUTISM

A thesis submitted in partial fulfillment of the requirements for the degree of Master of Science at the Medical College of Virginia Campus, Virginia Commonwealth University

By:

Nikhil N. Shah
B.S. Biological Sciences
Virginia Polytechnic Institute and State University
August, 2012

Advisor:
Lei Zhou, Ph.D.
Associate Professor
Department of Physiology and Biophysics

Virginia Commonwealth University
Richmond, VA
August 2017

ACKNOWLEDGEMENTS

First, I would like to thank Dr. Lei Zhou for his guidance and support since I became a student in the lab. His willingness to teach me molecular biology in a laboratory setting finally gave my biological science education the context that it was missing. His willingness to answer my questions and take the time to help ensure my understanding in our project made my experience memorable and has helped deepen my passion for science. His own relentless passion for science has truly inspired me to ask bigger questions and to think more scientifically, two qualities which will greatly help me in my future career as a doctor. I am forever grateful for the time I spent in his lab and I hope to work together with him again in the future.

Secondly, I would like to thank Vinay. His humble nature and constant willingness to help me out with my experiments is a testament to the kind person that he is. I can truly say without his presence in the lab, my experience would not have been as good as it was.

I would also like to thank Dr. Lui for all of her help during my Y2H investigation, as well as the time she took to thoroughly explain yeast genetics to me. The knowledge and skills I gained from her mentorship truly helped me understand my project better.

I would like to thank Dr. McGinn for being on my committee, and for being so understanding during the challenges I faced during the yeast two-hybrid investigation.

I would also like to thank Jian Bing ang Mungye for their friendship and help with the mice. Their kindness and spirits are indeed some of the best I've ever known.

I would also like to thank my good friends Terry and Waters for our epic group chats. Their unique sense of humor helped pass the time and always made me laugh, helping to keep me grounded during stressful times.

Finally, I want to thank my amazing wife who has supported me throughout this endeavor. Your love, understanding, and support remind me why I know we are perfect for each other.

Table of Contents

List of Tables

List of Figures

Abstract

SH3 AND MULTIPLE ANKYRIN REPEAT DOMAIN (SHANK3) AFFECTS THE EXPRESSION OF HYPERPOLARIZATION-ACTIVATED CYCLIC NUCLEOTIDE-GATED (HCN) CHANNELS IN MOUSE MODELS OF AUTISM

By Nikhil N. Shah

A thesis submitted in partial fulfillment of the requirements for the degree of Master of Science at the Medical College of Virginia Campus, Virginia Commonwealth University.

Virginia Commonwealth University, 2017

Major Advisor: Lei Zhou, Ph.D., Associate Professor
Department of Physiology and Biophysics

SH3 and multiple ankyrin repeat domains 3 (SHANK3) is a multidomain scaffold protein that is highly augmented in the postsynaptic density (PSD) of excitatory glutamatergic synapses within the central and peripheral nervous systems. SHANK3 links neurotransmitter receptors, ion channels, and other critical membrane proteins to intracellular cytoskeleton and signal transduction pathways. Mutations in SHANK3 are linked with a number neuropsychiatric disorders including autism spectrum disorders (ASDs). Intellectual disability, impaired memory and learning, and epilepsy are some of the deficits commonly associated with ASDs that result from mutations in SHANK3. Interestingly, these symptoms show some clinical overlap with presentations of human neurological disorders involving hyperpolarization-activated cyclin nucleotide-gated (HCN) channels. In fact, it has recently been demonstrated in human neurons that SHANK3 haploinsufficiency causes I_h-channel dysfunction, and that SHANK3 has a physical interaction with HCN channels via its ANKYRIN repeat domain. These insights

suggest that SHANK3 may play important roles in HCN channel expression and function, and put forward the idea that HCN channelopathies may actually encourage some of the symptoms observed in patients with SHANK-deficiency related ASDs. In this study, we provide preliminary data that suggests the ANK domain of SHANK3 interacts with COOH portion of HCN1. We also exploited the differences between two mouse models of autism to show that a subset of SHANK3 isoforms may be involved in the proper expression and function of HCN channels. We found that HCN2 expression is significantly decreased in a mouse model lacking all major isoforms of SHANK3 (exons 13-16 deleted; Δ13-16), while HCN2 expression is unaltered in a mouse model only lacking SHANK3a and SHANK3b (exons 4-9 deleted; Δ4-9). Surprisingly, we also found that HCN4 expression is altered in SHANK3$^{\Delta 13\text{-}16}$, but not SHANK3$^{\Delta 4\text{-}9}$. Taken together, our results show HCN channelopathy as a major downstream carrier of SHANK3 deficiency.

1 Introduction

1.1 An Introduction to Autism Spectrum Disorders

Autism spectrum disorder (ASD) presents as a developmental disability characterized by persistent deficits in social contexts involving communication and interaction, and patterns of repetitive behavior that restrict interests or activities (American Psychiatric Association, 2013). The diagnostic criteria for ASD is such that symptoms should be apparent in the early developmental stages of a child, and that these symptoms cause critical impairments in social situations, academic or occupational performance, and in any other relevant areas in which the expected level of functioning is compromised. Studies have shown that parents with autistic children observe developmental concerns with their child's communication and fine motor skills as early as six months after birth, and that the diagnostic stability of ASD in children as young as two years of age is often valid and binding (Bolton et al., 2012; Kleinman et al., 2008; Kozlowski et al., 2011; Lord et al., 2006). The severity of ASD is based on the person's level of impairment in social settings and the degree to which their behavior is restrictive and repetitive. Some illustrious examples of autistic behavior are as followed: delayed development of speech, echolalia, lack of interaction with other children or response to people, treating others as inanimate objects, extreme dislike of certain sounds or textures, aggressive behavior, desire to keep objects in specific physical patterns, and "islets of competence" – skills in which the person has advanced competence such as drawing, music, arithmetic, and memory.

1.1.2 ASD in the population

In the United States from 2006-2007, roughly 1 out of 6 children had a developmental disability such as speech and language impediments or more critical debilities such as intellectual deficits, cerebral palsy, and autism (Boyle et al., 2011). According to the Autism and Developmental Disabilities Monitoring Network, ASD affects approximately one out of every 68 children, and, although the disease is reported to occur in any race, ethnicity, or socioeconomic status, ASD is about 4.5 times more common in boys than girls in the United States (Boyle et al., 2011; Christensen, 2016). Interestingly, however, the severity of ASD-symptoms is more severe in females than in males (Frazier et al., 2014; Holtmann et al., 2007).

1.1.3 Risk factors for ASD

The risk factors and characteristics of ASDs are considerably broad. Many studies on twins have demonstrated that the concordance of ASD with monozygotic twins is greater than it is between dizygotic twins, and that vulnerability to ASD has a significant environmental factor in shared twin environments (Hallmayer et al., 2011; Rosenberg et al., 2009; Taniai et al., 2008). Parents who already have one child with ASD risk a higher recurrence rate (3-18%) of having another child with ASD (Ozonoff et al., 2011; Sumi et al., 2006), and parents with advanced age are also more likely to have a child with ASD (Durkin et al., 2008). Children who are born with low birth weights or prematurely are at a slightly greater risk of having ASD (Schendel and Bhasin, 2008). Interestingly, however, although autism is conventionally understood as having deficits

in social interactions and restrictive, repetitive behaviors, recent data reveals that roughly 44% of children diagnosed with ASD have average to above average intelligence as measured by intelligence quotient (IQ) tests (Christensen, 2016).

The susceptibility to ASDs is also higher in persons who have particular genetic or chromosomal abnormalities. Approximately one out of 10 children with autism will also present with down syndrome (DiGuiseppi et al., 2010), Fragile X syndrome (Kaufmann et al., 2004), tuberous sclerosis (Smalley, 1998), and neurometabolic disorders (Zecavati and Spence, 2009). Furthermore, the comorbidity of ASD and one or more developmental disorder diagnoses is a striking 83% while the co-occurrence of ASD with one or more psychiatric disorders or one or more neurological disorders is 10% and 16%, respectively (Levy et al., 2010). Some common developmental comorbidities are learning and intellectual disabilities, ADHD, sensory integration disorder, and various nonverbal learning disabilities (Christensen, 2016; Levy et al., 2010). Psychiatric comorbidities include disorders such as anxiety, bipolar, depression, obsessive-compulsive, psychosis, and schizophrenia (Simonoff et al., 2008). Neurological comorbidities include cerebral palsy, epilepsy and seizures, Tourette syndrome, encephalopathy, and loss of hearing or vision(Doshi-Velez et al., 2014; Levy et al., 2010).

1.1.4 ASD Etiology

Although a unified understanding for the causes of ASD is not known, it is well accepted among researchers that genetic abnormalities and environmental factors,

either individually or in combination, can manifest in disorders across the autistic spectrum. Significant progresses have been made in understanding the genetic causes of ASDs, largely due to whole genome and exome sequencing studies that have elucidated a number of genes implicated in syndromic and non-syndromic ASD (Hulbert and Jiang, 2016). This panorama of genes, which are mostly involved in synaptic function, cellular metabolism, remodeling chromatin, and translation of mRNA appear to unite in neuronal pathways that regulate brain homeostasis (Huguet et al., 2013). Indeed, some progress has been made in understanding the transmission of ASD in families. Simplex families (only one person affected with ASD) show a higher incidence of de novo mutations in comparison to affected individuals in multiplex families (Marshall et al., 2008; Sebat et al., 2007). This is in line with the high rate sporadic ASDs from de novo chromosomal mutations found in simplex families (O'Roak et al., 2011). Still, studies have suggested that subclinical autistic behaviors localized in multiplex families may imply unique mechanisms of genetic transmission of ASD among the population (Constantino et al., 2010; Virkud et al., 2009). Moreover, hereditary research on idiopathic ASDs culminates in the idea that, many different impairments of genes that link to common pathways may ultimately result in only damaging a select number of neurobiological pathways associated with development and plasticity (Chaste and Leboyer, 2012).

There is considerable evidence to support the hypothesis that ASDs are mainly a consequence of impairments in neuronal synapses and networks (Gilman et al., 2011; Zoghbi, 2003). The postsynaptic density (PSD) is a dense specialization of proteins localized to the postsynaptic membranes of excitatory neurons. Moreover, the PSD is

subjugated by glutamate receptors, a multitude of scaffold proteins including PSD95, Homer, etc., as well as signaling proteins (Sheng and Hoogenraad, 2007). Thus, PSD acts to aggregate and organize neurotransmitter receptors at the synaptic cleft, and also serves as a signaling apparatus (Kennedy, 1997, 2000; Ziff, 1997). The PSD plays a critical role in neuroplasticity as its size continually grows in proportion to the size and strength of neuronal synapses during long-term potentiation (Meyer et al., 2014). As there are many proteins in the PSD that are involved in the maintenance and regulation of synaptic function, many of their respective genes have been identified in ASDs that affect synaptic plasticity and neuronal development. Among some of the first candidate synaptic genes implicated in idiopathic ASDs were the X-linked neuroligins NLGN3 and NLGN4X, and the scaffolding protein SHANK3 (Durand et al., 2007; Gauthier et al., 2010; Jamain et al., 2003; Laumonnier et al., 2004; Moessner et al., 2007). Of these genes, SHANK3 remains among one of the most highly researched genes regarding ASDs. This is largely because SHANK3 haploinsufficiency has been implicated in monogenic forms of ASDs, affecting roughly 1% of the population (Moessner et al., 2007). The genetics, gene and protein structure, and implications of SHANK3 in ASD and ASD mouse models are discussed in detail next.

1.2 SHANK3

1.2.1 A brief introduction to SHANK3

SH3 and multiple ankyrin repeat domains 3 (SHANK3), also known as proline-rich synapse-associated protein (ProSAP2), is a multidomain scaffold protein belonging

to the SHANK family of proteins that is highly augmented in the PSD of excitatory glutamatergic synapses within the central and peripheral nervous system (Boeckers et al., 1999a, 2002). The cytogenic location of SHANK3 in homo sapiens is 22q13.33 and contains 58,570 base pairs of which 22 exons are translated into protein. Full-length Shank3 is comprised of 1,731 amino acids that fold into five highly conserved domains and facilitate protein-protein interactions: an ankyrin repeat (ANK), a Src homology 3 (SH3), a PSD-95/Discs large/ZO-1 (PDZ), a proline-rich region that contains Homer- and cortactin-binding sites (Pro-rich), and a sterile alpha motif (SAM; Sheng and Kim, 2000; Wang et al., 2014a; Fig 1). The transcription of SHANK3 is considerably elaborate as the gene possesses at least six intragenic promoters and undergoes alternative splicing, resulting in an impressive array of protein isoforms (Lim et al., 1999; Waga et al., 2014; Wang et al., 2014b; Zhu et al., 2014). SHANK3a, the full-length isoform, contains all five functional domains while the rest of the cohort is produced by alternative splicing and different promoter-specific regions within the SHANK3 gene. Accordingly, these other isoforms (e.g. SHANK3b/c/d/e/f) encompass varying arrangements of the five different functional domains (Wang et al., 2014a).

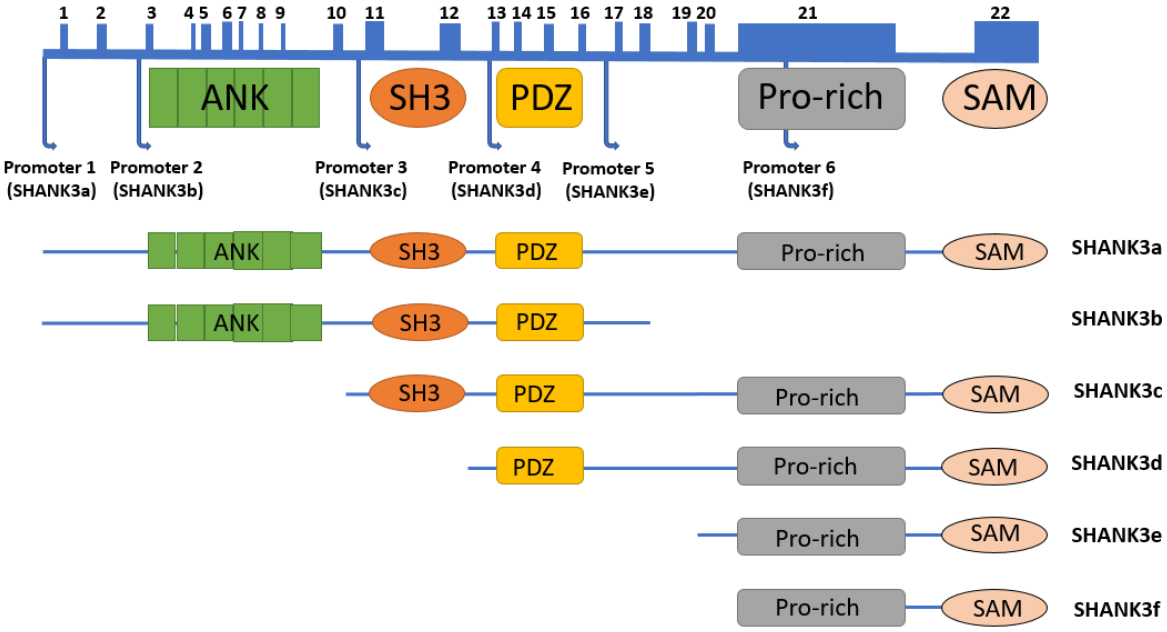

Figure 1. Cartoon of Shank3 gene organization and the domain composition within major Shank3 isoforms. Shank3 has 22 exons, of which 11, 12, 18, 21, and 22 undergo alternative splicing (Wang et al., 2014b). The six intragenic promoters help develop an array of isoforms (Shank3a-f), each composed of different combinations of functional domains. Note that, as the genetics of Shank3 becomes more understood (e.g. alternative splicing, new promoters) a complete list of Shank3 isoforms remains to be determined. Image adapted from (Wang et al., 2014b).

1.2.2 Expression of SHANK3

SHANK3 is expressed in various tissues throughout the body such as fat, kidney, lung, spleen, heart, and brain (Fagerberg et al., 2014). In the brain in particular, it is becoming more evident that SHANK3 isoforms show differential expression patterns not only among different brain regions but in development as well (Wang et al., 2014a). For example, q-PCR studies in mouse brains show SHANK3a expression increases significantly after postnatal day five and stabilize at postnatal day 10 while SHANK3b expression increases steadily from postnatal day one until four weeks when it stabilizes (Wang et al., 2014a). Region specific characterizations of SHANK3 in mice brains have also indicated variable expression levels of selective SHANK3 isoforms; the expression of full-length SHANK3a, SHANK3b, and SHANK3e are highest in the striatum vs other brain compartments; SHANK3c and SHANK3d are expressed more in the cerebellum vs. other brain compartments; messenger RNA is highly abundant for all isoforms in hippocampal neurons but not in hippocampal astrocytes (Monteiro and Feng, 2017; Wang et al., 2014a). Moreover, it appears that varying mutations in SHANK3 can affect the function of select SHANK3 isoforms, and, consequently, each impairment may result in idiosyncratic disruptions at specific excitatory synapses in different regions of the brain, thus providing some explanation for the diversity of phenotypes seen in ASDs caused by mutations in SHANK3 (Monteiro and Feng, 2017; Wang et al., 2014a).

1.2.3 The Role of SHANK3 in the Postsynaptic Density

As SHANK3 is a scaffolding protein, the protein-dense nature of the PSD where it is primarily localized allows for intensive protein-protein interactions and complex synaptic functions. To begin with, it is conventionally known that SHANK3 is involved in glutamate receptor clustering. Metabotropic glutamate receptor 5 (mGluR5) is a G Protein-coupled receptor involved in neurotransmission and the maintenance of normal brain function. The interaction between SHANK3 and mGluR5 is mediated by the proline rich domain of SHANK3, which binds with the mGluR-binding protein Homer (Tu et al., 1999). One study showed that RNA interference of SHANK3 in cultured neurons decreased the synaptic levels of mGluR5 and resulted in decreased mGluR5-dependent neurotransmission and synaptic plasticity, and that the use of a positive allosteric modulator rescued mGluR5 signal transmission (i.e. the study revealed mGluR5 as a potential target for pharmacological therapies in patients with ASD; Verpelli et al., 2011). Another study demonstrated in a mutant SHANK3 mouse line that SHANK3 deficiency impairs mGluR5-Homer scaffolding, which has been implicated in ASD phenotypes such as learning deficits (Wang et al., 2016).

Guanylate kinase-associated protein (GKAP) and postsynaptic density-95 (PSD95) complexes mediate the interaction between the PDZ domains of SHANK3 and *N*-methyl-D-aspartic acid receptor (NMDAR) while the PDZ domain directly interacts with α-amino-3-hydroxyl-5-methyl-4-isoxazole-propionic acid receptor (AMPAR) (Boeckers et al., 1999b; Ehlers, 1999; Kim et al., 2009; Naisbitt et al., 1999; Tu et al., 1999; Uchino et al., 2006). NMDAR, AMPAR, and kainate receptors are the three major ionotropic glutamate receptors. Briefly, NMDARs are calcium permeable ionotropic glutamate receptors that only open in response to glutamate binding when the neuronal

membrane potential is depolarized. NMDARs are highly involved in memory and synaptic plasticity because activation NMDARs can induce long-term potentiation (LTP) or long-term depression (LTD; Hasan et al., 2013; Sheng and Kim, 2002; Shipton and Paulsen, 2014). Indeed, mutations in these glutamate receptors have been linked to ASDs (Carlson, 2012). Although the mechanism through which SHANK3 regulates the expression and function of NMDAR remains largely unknown, it has been shown that loss of SHANK3 in mice induces decreased function of NMDAR by obstructing the Rac1/PAK/Cofilin/actin signaling pathway (Duffney et al., 2013).

As mentioned, SHANK3 has a direct interaction with AMPARs via its PDZ domain by binding to the carboxylic acid terminus of the receptor (Uchino et al., 2006). Briefly, AMPARs activate in response to glutamate binding which facilitates rapid synaptic transmission in the central nervous system. Like NMDARs, AMPARs are also intimately involved in synaptic plasticity via LTP and LTD (Song and Huganir, 2002), and these receptors play a critical role in the formation of epileptic seizures (Rogawski, 2013). It has recently been found that SHANK3 interacts with Rho-GAP interacting CIP4 homolog 2 (Rich2), and that these binding partners together regulate the recycling of AMPARs and increase the dendritic spines of hippocampal neurons in mice, linking the SHANK3-Rich2 interaction to synaptic plasticity (Raynaud et al., 2013).

SHANK3 also plays a critical role in the organization of actin cytoskeleton and the development of dendritic spines (Sala et al., 2001). In fact, re-introduction of SHANK3 can rescue spinogenesis in aspiny neurons in hippocampal neurons (Roussignol et al., 2005). SHANK3 requires several actin-regulatory binding partners in order to substantiate the maintenance and formation of excitatory synapses. For

example, SHANK3 interacts with cortactin via its Pro-rich domain. Cortactin is an F-actin binding protein that plays a key role in stabilizing the branching of actin filaments (Weaver et al., 2001). Cortactin requires the Arp2/3 actin polymerization complex to bind a nucleate new branches of actin (Uruno et al., 2001). It has recently been suggested that Shank proteins recruit cortactin to the synapses and that their interaction is involved in the maintenance and function of neuronal spine flexibility (MacGillavry et al., 2016). However, although mutations in SHANK3 affect the levels of F-actin, they do not appear to affect levels of cortactin in dendritic spines (Durand et al., 2012). Alpha fodrin (α -fodrin, formally known as SPTAN1) also mediates the interaction between SHANK3 and the actin cytoskeleton (Böckers et al., 2001). Interestingly, the binding of the ANK repeat domain in SHANK3 to α -fodrin may be regulated by a novel, conserved domain termed the Shank/ProSAP -N-terminal (SPN) domain, located N-terminal to the ANK repeat domain (Mameza et al., 2013). The ANK repeat domain also connects SHANK3 to the actin cytoskeleton by binding to Sharpin, which has been associated with the multimerization of Shank proteins (Lim et al., 2001). Other actin binding partners for Shank include Abp1 (actin binding protein 1) that directly links the Pro-rich region of SHANK3 to F-actin (Qualmann et al., 2004); beta PIX, a guanine nucleotide exchange factor for the small GTPases Rac1 and Cdc42, which is recruited by Shanks to modulate postsynaptic structure (Park et al., 2003); and ProSAPiP1 (ProSAP-interacting protein 1), which links the PDZ domain of SHANK3 to Spine-associated Rap-Gap (SPAR) and is highly involved in the regulation of dendritic spine morphology (Wendholt et al., 2006). Moreover, the complexity of SHANK3's role in the PSD

continues to increase in light of the fact that the array of SHANK3 isoforms likely undergo differential interactions with a multitude of PSD-localized binding partners.

1.2.4 Mutations in SHANK3 Can Result in ASDs

Mutations in SHANK3 have been associated with individuals affected with ASD for over a decade now (Durand et al., 2007; Gauthier et al., 2009; Moessner et al., 2007). The 22q13.3 deletion syndrome (Phelan-McDermid Syndrome; PMS) involves the monogenic microdeletion of SHANK3 in roughly 95% of the cases, in which more than half of the patients show autistic-like behavior (i.e. patients have a syndromic form of ASD; Phelan and McDermid, 2012). PMS is characterized by global developmental delay, speech impairments, intellectual disabilities, hypotonia, and ASD-like behaviors. Although monogenic forms of autism caused by point mutations in exons or intragenic mutations in SHANK3 only account for a small fraction of ASDs, these cases establish haploinsufficiency of SHANK3 as sufficient for pathogenesis (Berkel et al., 2010, 2012; Boccuto et al., 2013; Moessner et al., 2007; Wang et al., 2014b). In fact, all reported cases of SHANK3 deletions associated with ASD are heterozygous in nature (Moessner et al., 2007). Still, recurrent breakpoints during chromosomal translocation in the SHANK3 gene have also been reported (Bonaglia et al., 2006).

1.2.5 Mouse Models of Autism

Modeling SHANK mutations in humans through the use of mutant mouse lines has received considerable attention over the last decade. At present, there are 11 lines

of mutant mice with each carrying a different mutation in the SHANK3 gene. These mutations are deletions of different exons and thus result in the loss of functional domains in SHANK isoforms. They are as followed: Δe4-9$^{Buxbaum(B)}$ (Bozdagi et al., 2010), Δe4-9$^{Jiang(J)}$ (Wang et al., 2011b), Δe4-7 (Peça et al., 2011), Δe9 (Lee et al., 2015), Δe11 (Schmeisser et al., 2012), Δe13-16 (Peça et al., 2011), Δe21 (two lines; Duffney et al., 2015; Kouser et al., 2013), Δe21^{R1117X} (Zhou et al., 2016), Δe21InsG (Speed et al., 2015), and Δe4-22 (Wang et al., 2016). All of these mutations result in a frameshift of the downstream transcripts and thus truncated SHANK3 proteins and isoforms. It is important to note however that, given how SHANK3 possesses six intragenic promoters and undergoes alternative splicing of exons, each of these mice display select impaired isoforms but not the entire disruption of the SHANK3 (Wang et al., 2014b; Zatkova et al., 2016).

Accordingly, each of these mice present with different synaptic structures and behavioral phenotypes. For example, in Δe4-9$^{Buxbaum(B)}$ mice, Bozdagi and colleagues observed a reduction of the signal transmission at glutamatergic synapses, impairment of LTP, and deficits in social interaction and communication (Bozdagi et al., 2010). However, in Δe4-9$^{Jiang(J)}$ mice, signal transmission in CA1 hippocampal neurons is unaffected, but LTP is reduced (Wang et al., 2011b). Wang and colleagues also observed decreased levels of PSD proteins and altered dendritic spine morphology, as well as aberrations in social and motor behaviors, ultrasonic vocalizations, and learning and memory (Wang et al., 2011b). Profound ASD-like phenotypes are observed in Δe13-16 mice. Abnormal, repetitious grooming which lead to skin lesions was observed, as well as increased anxiety and a predilection for social novelty (Peça et al., 2011).

Interestingly, these mice also showed impairments at cortico-striatal synapses, a facet of neural circuitry hypothesized to be dysfunctional in ASDs (Fuccillo, 2016; Peça et al., 2011). Many behavioral tests on Δe21 mice were normal, although some ASD-like phenotypes (such as grooming and impaired spatial learning) were observed (Kouser et al., 2013). Still, electrophysiological studies on these mice revealed debilities in plasticity and synaptic transmission in the hippocampus, which is consistent with their observed spatial learning deficiency (Kouser et al., 2013). Because the mouse model Δe4-22 mouse line created by Jiang and colleagues mimics the genetic defect most frequent among patients with ASD (i.e. loss of the entire SHANK3 gene), it is, so far, perhaps the model with the most construct validity. (Wang et al., 2016). Interestingly, the loss of SHANK3 in these mice leads to the reorganization of Homer and mGluR5 at both the synapse and soma, revealing a neuropathology mechanism may be present among humans with ASD (Wang et al., 2016).

1.2.6 Rescuing Phenotypes in ASD Mouse Models

Impressively, recent studies have shown to be successful in rescuing ASD-phenotypes in mice models of autism and may provide insight into pharmacological therapies for ASD patients. By inhibiting cofilin (an actin depolymerizer) and activating Rac1, researchers rescued physiological and behavioral impairments in mutant SHANK3 mice (Duffney et al., 2015). Re-expression of the SHANK3 gene in a mouse model with conditional SHANK3 knock-in enhanced PSD proteins, dendritic spines, and striatal function (Mei et al., 2016). Although some behavioral phenotypes were rescued in these mice, such as repetitious grooming and impaired social interaction, adult mice

still demonstrated anxiety and poor motor coordination (Mei et al., 2016). Indeed, substantial effort will be required to fully characterize the relationship between the array of ASD phenotypes and the genetic complexity of SHANK3 mutations. Nonetheless, it appears that different mutations of SHANK3, which affect SHANK3 isoforms differentially, results in a panorama of ASD phenotypes. Linking these phenotypes to the molecular diversity in SHANK3 mutations presents an incredible challenge.

1.3 HCN Channels

1.3.1 A Brief Overview of the Structure of HCN Channels

Hyperpolarization-activated cyclin nucleotide-gated (HCN) channels are a subgroup of cyclic nucleotide-regulated cation channels within the superfamily of poor-loop cation channels (Yu et al., 2005). The currents carried by HCN channels are hyperpolarization-activated currents (I_h; also known as I_f for “funny” current), and were first observed in 1976 in rabbit heart (Noma and Irisawa, 1976). In mammals, this small family of membrane proteins is comprised of four members (HCN1-4) that are expressed in cardiac and nervous tissue. Each HCN channel is composed of four subunits arranged such that they form a homo- or heterotetramers with a centrally located pore. Each of these four subunits have characteristic biophysical signatures such as hyperpolarization-dependent activation, mixed permeability for Na+ and K+ ions that results in a reversal potential around -30 to -40 mV, and sensitivity to intracellular cAMP and cGMP (Gauss et al., 1998; Ishii et al., 1999; Jiang et al., 2008; Ludwig et al., 1998, 1999; Moosmang et al., 2001; Santoro et al., 1998; Seifert et al., 1999). HCN

channels can be broken down into three structural segments: a cytosolic amino (NH_2) terminal portion, the transmembrane core section, and cytosolic carboxylic acid (COOH)terminal domains. The transmembrane core is comprised of six α-helical segments (S1-S6) with a positively charged S4 segment serving as the voltage sensor, a trademark of the voltage-gated cation channel superfamily (Chen et al., 2000; Vaca et al., 2000; Yu and Catterall, 2004; Fig 2). However, the inward movement of the positively charged S4 segment within the core of the channel has contrasting effects between HCN and other depolarizing channels, activating HCN channels and deactivating, for example, Kv channels (Seoh et al., 1996). Although these ion channels structurally resemble K+ channels, they are less selective for K+ ions and also permit the inward flow of Na+ ions (Craven and Zagotta, 2006). The COOH-terminal of all HCN channels possesses two structural domains, the cyclic nucleotide binding domain (CNBD) and a C-linker region that links this COOH-terminus to the transmembrane core. As discussed in detail below, a unique feature of HCN channels is the presence of a CNBD domain that moderates the effect of cAMP or cGMP on HCN channels (Chen et al., 2001; Wainger et al., 2001). Between the four channels, there is high sequence homology between the transmembrane pores and the proximal segments of the COOH-termini while the sequences of the NH2-termini and the distal COOH-termini share little homology (Biel et al., 2002, 2009; Kaupp and Seifert, 2001). Accordingly, allosteric interactions between the transmembrane segments and the proximal portion of the COOH-terminus occur during channel gating.

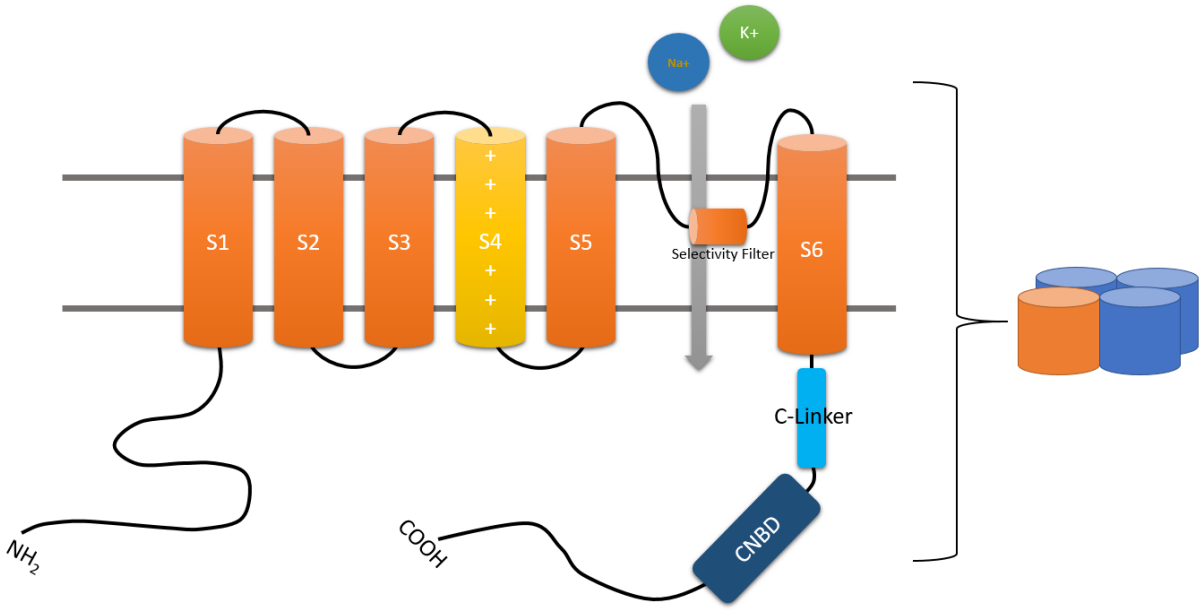

Figure 2. Cartoon Schematic of an HCN Channel. HCN channels are composed of four subunits that combine to form a central pore within the membranes of neurons in the nervous and cardiovascular systems. Each subunit has six transmembrane segments (S1-S6) of which S4 acts as the voltage sensor. HCN channels are unique in that they are less selective to K+ ions and permit the flow of Na+ ions as well. This unique selectivity filter is located between S5 and S6. The C-terminal of HCN channels is also unique in that it possesses a cyclic nucleotide binding domain (CNBD) to which cAMP is able to bind and shift the $V_{1/2}$ of HCN1,2, and 4.

1.3.2 HCN Channels are Activated by Hyperpolarization

As their name suggests, HCN channels activate upon hyperpolarization. These channels conduct hyperpolarization-activated cation currents (I_h) which, in contrast to most ion channels that conduct upon membrane depolarization, allow the inward flux of cations inward upon membrane hyperpolarization. Conversely, depolarization of the membrane closes HCN channels, which impedes the tonic inward flux and has the ultimate effect of hyperpolarizing the membrane back towards its RMP. HCN channels are partially active near the resting membrane potential (RMP) and thus influence the membrane potential to stabilize at more depolarized voltages (Doan and Kunze, 1999; Ludwig et al., 2003; Lupica et al., 2001; Meuth et al., 2006). Hence, at physiological conditions, HCN channels have a reversal potential at roughly 0 to -40 mV (DiFrancesco, 1993). In general, the gating kinetics of HCN channels can be characterized by two currents upon activation: a minor instantaneous current (I_{INS}), which presents almost immediately, and a major slowly developing current (I_{SS}) that stabilizes from a range of tens of milliseconds to seconds (Macri and Accili, 2004; Proenza et al., 2002). The most functionally significant attributions of I_h currents are the generation and regulation of the heart beat (i.e. “pacemaker” currents; Brown et al., 1979b; DiFrancesco et al., 1989), and control of intrinsic, rhythmic oscillations in neuronal circuitry (Dossi et al., 1992; Leresche et al., 1990, 1991; McCormick and Pape, 1990). At the cellular level, HCN channels contribute to the maintenance of resting membrane potential, regulation of input resistance, and the initiation and propagation of action potentials.

1.3.3 HCN Channel Activity Can Be Modulated by cAMP

As indicated by their name, one of the key characteristics of HCN channels is their ability to be modulated by the direct binding of cyclic nucleotides (DiFrancesco and Tortora, 1991; Ludwig et al., 1998; Wainger et al., 2001). This feat is unique to HCN channels as most of the functional roles mediated by cAMP are through protein phosphorylation (Duman and Nestler, 1999). Elevated levels of cAMP significantly increase the activation kinetics of HCN channels by shifting the voltage-dependence of the channel to more positive membrane potentials, especially HCN2 and HCN4 (Bobker and Williams, 1989; Wainger et al., 2001). Contrarywise, decreased levels of cAMP reduce HCN channel activation and shift the membrane potential to more negative values. This regulation of cyclin nucleotides has significant physiological contributions such as the “fight or flight” mechanism. For example, β-adrenergic agonists, which increase cAMP levels, results in an increased heart rate (Brown et al., 1979b, 1979a), while muscarinic acetylcholine receptor agonists result in the deceleration of the heart (DiFrancesco and Tromba, 1988a, 1988b; DiFrancesco et al., 1989).

1.3.4 Basic Physiology of HCN Channels

Although HCN channels are highly implicated in the proper function of SAN cells and Purkinje fibers in cardiac tissues (DiFrancesco, 1993), the focus in this thesis will be more directed towards their physiological significance in the central nervous system. As mentioned, HCN channels are partially open at rest and, consequently, they help set and stabilize the RMP. This membrane stabilization occurs because constant

conductance of an inward cation current decreases the membrane resistance (R_m), which is generally described as the ratio of the change in voltage to the current propagated (Nolan et al., 2007). In this way, HCN channels act as physiological voltage clamps as they compete against hyperpolarizing and depolarizing currents; they activate upon hyperpolarization and close when the membrane depolarizes, respectively (Bayliss et al., 1994; Biel et al., 2009; Mayer and Westbrook, 1983; Nolan et al., 2007; Solomon and Nerbonne, 1993). These phenomena can be seen in voltage clamp experiments and are termed “voltage sags.” Depolarizing voltage sags can be seen by eliciting a hyperpolarization current step, which increases the number of I_h currents and eventually shifts the membrane potential back towards the RMP (Biel et al., 2009; Pape, 1996; Robinson and Siegelbaum, 2003). Likewise, Hyperpolarizing voltage sags can be seen by eliciting depolarizing current steps, which halts the tonic I_h current and drags the membrane potential back down towards its resting potential (Biel et al., 2009; Pape, 1996; Robinson and Siegelbaum, 2003). The HCN channels opposition to hyperpolarizing or depolarizing inputs also has the effect of preventing low-frequency oscillations in the membrane potential (Nolan et al., 2007). Moreover, the consequences of this type of channel conductance behavior is that, because I_h currents are typically active at RMP, the input resistance of the neuron is already lessened, and any currents arriving at the synapse will have diminished effects on the membrane potential (also known as the “dampening effect”). Therefore, the amplitude and kinetics of excitatory postsynaptic potentials (EPSPs) are decreased. Similarly, the effects of inhibitory postsynaptic potentials (IPSPs) are negated because hyperpolarization

activates the channel and permits cation conductance, thus depolarizing the membrane (Atherton et al., 2010; Kase and Imoto, 2012).

Dendritic integration is the process by which neuronal cells take excitatory and inhibitory synaptic inputs and integrate this information at the soma in order to determine whether or not an action potential (AP) will fire. Dendritic integration has been well characterized in CA1 pyramidal neurons (Stuart and Spruston, 2015), and this process is heavily reliant upon HCN channels for a unique type of regulation (Magee, 1998, 1999, 2000). For example, it is generally anticipated that repetitious EPSPs generated at more distal dendrites undergo summation in the soma to elicit an AP. However, temporal summation due to EPSPs distal to the soma are often not present in neocortical and hippocampal pyramidal neurons. This phenomena is explained by an increasing somatodendritic axis gradient of HCN channels such that the concentration is lower in the soma and increases roughly 10-fold along the way to distal dendrites (Biel et al., 2009; Lörincz et al., 2002; Magee, 1998, 1999, 2000). The physiological consequence of this is that the input resistance at dendritic sites is significantly reduced, which results in smaller voltage changes by incoming EPSPs. Moreover, although HCN channels tend to shift the potential of the membrane to a more depolarized state, it appears that the large collections of channels at dendritic sites has the principal effect of diminishing input resistance and EPSP summation, predominantly in the neurons of the cortex and hippocampus (Berger et al., 2001; Magee, 1998, 1999, Poolos et al., 2002, 2006; Williams and Stuart, 2000). However, HCN channel localization (at lower concentrations) in the soma of non-pyramidal interneurons of the cortex and hippocampus has been characterized as well (Lupica et al., 2001). Yet, the overall

result is still inhibitory as any depolarization will halt the flux of I_h currents and have a hyperpolarizing effect on the membrane. Moreover, the global excitability of the neurons in the cortex and hippocampus is essentially weakened due to the dichotomic functionality of HCN channels.

1.3.5 Differences among HCN Isoforms

As mentioned, there are differences among HCN channels with respect to gating kinetics of activation and inactivation, steady-state voltage dependency, and degree of influence by cAMP. For example, HCN1 has the fastest gating kinetics (Ishii et al., 2001; Santoro et al., 2000), the most positive $V_{1/2}$ value (i.e. more HCN1 channels are active at RMP than the other isoforms; Altomare et al., 2003; Baruscotti et al., 2005), and presents the weakest shift in activation curve in saturating cAMP conditions (Altomare et al., 2003; Viscomi et al., 2001; Wainger et al., 2001; Wang et al., 2001). Although HCN2 and HCN4 both demonstrate intense sensitivity to cAMP and have relatively equal $V_{1/2}$ values (Altomare et al., 2003; Ludwig et al., 1999; Moroni et al., 2000; Viscomi et al., 2001; Wainger et al., 2001; Wang et al., 2001; Zagotta et al., 2003), both channels have slower opening kinetics than HCN1, especially HCN4 being the slowest of the four isoforms (Ishii et al., 1999; Ludwig et al., 1999; Seifert et al., 1999). HCN3 channels in humans have intermediate activation kinetics, and surprisingly, even though the channel possesses a CNBD, the channel elicits no functional response upon the binding of cyclic nucleotides (Stieber et al., 2005; Table 1).

	Amino Acids	Activators	Inhibitors	V1/2	ΔV1/2 with cAMP	T act
HCN1	890	cAMP > cGMP (both weak)	Cs+, ZD7288, ivabradine	-70 to -90 mV	2 to 7 mV	30 to 300 ms
HCN2	889	cAMP > cGMP	Cs+, ZD7288, ivabradine	-70 to -90 mV	10 to 25 mV	150 ms to 1 s
HCN3	774	none	Cs+, ZD7288, ivabradine	-80 to -95 mV	n/a	250 to 400 ms
HCN4	1203	cAMP > cGMP	Cs+, ZD7288, ivabradine	-70 to -90 mV	10 to 25 mV	Hundreds of ms to seconds

Table 1. General Features of the HCN Channel Family. The data was organized into this chart based on the information provided in the excellent review done by (Biel et al., 2009). Amino acid numbers were taken from Uniprot and represent the human HCN isoforms. T act stands for “time for activation.”

1.3.6 The Expression of HCN Isoforms in the Nervous System

HCN1-4 are all expressed in the brain, albeit they have different expression patterns and localizations within the nervous system (Monteggia et al., 2000; Moosmang et al., 1999; Santoro et al., 2000); HCN1 expression has been observed in the spine, brainstem, neo and cerebellar cortex, and hippocampal tissues (Milligan et al., 2006; Moosmang et al., 1999; Notomi and Shigemoto, 2004; Santoro et al., 1997); HCN2 is expressed more so in the thalamus and brainstem compartments, although its distribution in the brain is global (Milligan et al., 2006; Moosmang et al., 1999; Notomi and Shigemoto, 2004; Santoro et al., 2000); HCN3 expression is considerably low throughout the central nervous system (Moosmang et al., 1999; Notomi and Shigemoto, 2004; Stieber et al., 2005); HCN4 expression is variable among different brain compartments, having pronounced mRNA levels in the mitral cell layer of the olfactory bulb and the thalamus, but little expression in the cerebral layers (Ludwig et al., 1998; Moosmang et al., 1999; Notomi and Shigemoto, 2004; Santoro et al., 1997, 2000).

1.3.7 HCN Channels and Memory

More recently, HCN channels have been implicated in working memory and age-related working memory decline **(Wang et al., 2007, 2011a)**. Briefly, working memory is a limited, temporary cognitive organization of information in the prefrontal cortex that is responsible for reasoning and decision-making behavior. The role of HCN channels in working memory is described as follows: During a wake cycle, alertness causes low levels of norepinephrine (NE) to be released. NE activates α_{2A}-adrenoceptors, which

halts the production of cAMP. This results in a decreased number of HCN channels open at the RMP, which increases the input resistance of the membrane and thus the effect of synaptic activity on synapses. Moreover, reduced HCN channel activity may allow for increased neuronal firing to relevant spatial information (Wang et al., 2007). On the other hand, D1- receptors increase cAMP production (Vijayraghavan et al., 2007). Thus, when HCN channels are activated, the input resistance of the membrane decreases because the open probability of the channels is higher due to the effects of cAMP. In this way, HCN channels may help inhibit irrelevant spatial information.

1.3.7 HCN Channels and Neurological Disorders

HCN channels have been indicted for having at least some role in neurological disorders such as epilepsy, neuropathic pain disorders and Parkinson's disease. Down regulation of I_h currents has been attributed to epileptogenesis and spontaneous absence seizures in mice with mutant HCN1 and HC2, respectively (Chung et al., 2009; Huang et al., 2009; Ludwig et al., 2003). However, transcriptional channelopathies of HCN channels have also shown to be related with epileptogenesis and seizure production. For example, in mice models of epilepsy it was discovered that the altered expression of HCN1 was associated with the incidence of seizures (Kole et al., 2007; Phillips et al., 2014), and that alterations of HCN1 and HCN2 expression in young mice enhance the tendency to develop epilepsy in adult mice (Brewster et al., 2002; Dube et al., 2000). This is also consistent with the alterations in HCN channel expression observed in human epileptic brain tissue (Bender et al., 2003). Surprisingly, only a few studies have confirmed HCN channels as the direct cause of epilepsy in humans

(DiFrancesco et al., 2011; Nakamura et al., 2013; Nava et al., 2014; Tang et al., 2008). There is increasing evidence implicating HCN channels mediating the initiation and frequency of APs in neural pathways involved in pain (Jiang et al., 2008). Neuropathic pain can be described as an enduring state of pain due to nerve tissue damage. A study has demonstrated that the HCN2 isoform appears to maintain neuropathic pain succeeding nerve damage (Momin et al., 2008). Interestingly, in mice with HCN2 deletions specifically in sensory nociceptors, researchers have found that neuropathic pain can be abolished without affecting the response to ordinary acute pain (Emery et al., 2011). Moreover, developing pharmacological therapies to target HCN channels presents a significant challenge given the critical functionality of the HCN channel family within the central nervous system. The indictment of HCN channels in Parkinson's disease is also very recent, and only a handful of studies have characterized I_h in the substantia nigra during the atrophy of dopaminergic neurons, the chief etiology of Parkinson's disease. Although little is known about how downregulation of I_h is associated with Parkinson's disease, loss of channel activity appears to follow after the degeneration of dopamine neurons (Chan et al., 2011; Good et al., 2011).

1.4 SHANK3-HCN Interactions

It has recently been suggested by several studies that there is some clinical overlap between the symptoms of neurological disorders involving HCN channels and the symptoms of ASDs associated with SHANK3 haploinsufficiency. In fact, it has recently been demonstrated in human neurons that SHANK3 haploinsufficiency results

in I_h-channel dysfunction because of decreased current density, and that SHANK3 deletion results in decreased levels of endogenous HCN3 and HCN4 proteins (Yi et al., 2016). Yi et al. also observed in pulldown assays that SHANK3 has a physical interaction with HCN1, HCN2, and HCN3 channels via its ANKYRIN repeat domain. These insights suggest that SHANK3 may play important roles in HCN channel expression and function, and that HCN channelopathies (I_h-current impairments) may actually encourage some of the symptoms observed in patients with ASDs caused by mutations in SHANK3 and in Phelan-McDermid syndrome (Yi et al., 2016). Further, our lab has recently characterized thalamocortical neurons in two different ASD mouse models, SHANK3$^{\Delta 13\text{-}16}$ and SHANK3$^{\Delta 4\text{-}9}$ (Bozdagi et al., 2010; Peça et al., 2011), and found that I_h-current impairment is largely responsible for changes in the basic neuronal electrical properties of SHANK3 deficient neurons (not yet published). SHANK3$^{\Delta 13\text{-}16}$ mice, but not SHANK3$^{\Delta 4\text{-}9}$ mice, exhibited decreased membrane potential and an increase in input resistance, trademarks of HCN channelopathy (Baruscotti et al., 2010; Poolos, 2012). Although the targeted mutations in SHANK3$^{\Delta 4\text{-}9}$ result in the loss of full-length SHANK3 (SHANK3a) and SHANK3b isoforms, these mice still retain one major of SHANK3 protein isoform, SHANK3c (Bozdagi et al., 2010; Wang et al., 2014b). Therefore, we suspect that this remaining isoform may help preserve the usual expression of HCN channels in SHANK3$^{\Delta 4\text{-}9}$ mice. On the other hand, SHANK3$^{\Delta 13\text{-}16}$ mutations result in the loss of most SHANK3 isoforms, thus explaining the difference in the neuronal electrical properties between these two mouse models (Peça et al., 2011; Wang et al., 2014b).

1.5 Goal of This Work

The goal of this work was to investigate potential interactions between functional SHANK3 domains and the N- and C- Termini of HCN channel isoforms, and to further characterize the protein expression profiles of HCN isoforms in SHANK3$^{\Delta 13\text{-}16}$ and SHANK3$^{\Delta 4\text{-}9}$ mice. Our central hypothesis for this study is that the HCN channelopathy plays a major role downstream from SHANK3 deficiency, especially in altering the basic electrical properties (i.e. RMP and the input resistance) of affected neurons. Our preliminary data suggests that SHANK3 interacts with the C-terminus of HCN1. We also demonstrate that the differences between targeted mutations of SHANK3 in mouse models of autism have drastically opposing effects on the expression of HCN channels. Therefore, we propose that a subset of SHANK3 isoforms are necessary for the proper expression of certain HCN channels.

2 Methods

2.1 Yeast Two-hybridization

Five cDNA fragments encoding different amino acid segments of SHANK3 [amino acids (aa) 1-353 (ankyrin containing), 348-668 (SH3 and PDZ containing), 663-1000 (Pro-rich containing), 994-1338 Pro-rich and homer binding site containing), and 1338-1730 (SAM containing)] were inserted in pGBKT-7 to yield the following plasmids to be used as bait: pGBKT7_SHANK3-1, pGBKT7_SHANK3-2, pGBKT7_SHANK3-3, pGBKT7_SHANK3-4, and pGBKT7_SHANK3-5. Four cDNA fragments encoding various amino acid segments of the N- and C-termini of mouse HCN1 [aa (HCN1 N-terminus containing), (HCN1 CNBD domain containing), (HCN1 distal C-terminus containing), and (HCN1 distal C-terminus without the final SNL aa)] were inserted in pGADT-7 to yield the following library plasmids: pGADT7_m1-N, pGADT7_m1-C, pGADT7_m1-CNBD, pGADT7_m1-ext-C, and pGADT7_m1-ext-C_noSNL. Five cDNA fragments encoding various amino acid segments of the N- and C-termini of mouse HCN2 [aa (HCN2 N-terminus containing), (HCN2 C-terminus containing), (HCN2 CNBD domain containing), (HCN2 distal C-terminus containing), and (HCN2 distal C-terminus without the final SNL aa)] were inserted in pGADT-7 to yield the following plasmids: pGADT7_m2-N, pGADT7_m2-C, pGADT7_m2-CNBD, pGADT7_m2-ext-C, and pGADT7_m2-ext-C_noSNL. After creating cDNA constructs for the PDZ and SH3 domains, we inserted them in pGBKT7 plasmids to create pGBKT7_SHANK3-PDZ and pGBKT7_SHANK3-SH3. Upon the realization that the PDZ and pro-rich fragments within the pGBKT7 plasmids resulted in autoactivation, we inserted new cDNA

constructs into pGADT7 plasmids to create pGADT7_SHANK3-PDZ and pGADT7_SHANK3-pro-rich. Likewise, we inserted new cDNA constructs of the CNBD and Ext-C of the mHCN2 into pGBKT7 plasmids to create pGBKT7_m2-CNBD and pGBKT7_m2-ext-C. For controls, we used the pGBKT7-53 (which encodes the Gal4 DNA binding domain fused with murine p53) and pGADT7-T (which encodes the Gal4 activation domain fused with SV40 large T-antigen) matchmaker vectors (Clontech Laboratories, Inc.). The bait and prey plasmids were co-transformed into the yeast train AH109. Detection of successful transformation was done by observing colony growth on yeast synthetic media with depleted leucine and tryptophan. Detection of protein-protein interactions was done by observing growth on yeast synthetic media with either depleted leucine, tryptophan, and histidine (triple dropout media), or depleted leucine, tryptophan, histidine, and adenosine (quadruple dropout media). All cDNA constructs were verified by DNA sequencing. Yeast transformation protocols were followed as directed by Clontech Laboratories, Inc. Matchmaker® Gold Yeast Two-Hybrid System User Manual.

SHANK3 and HCN2 Knockout mice

Shank3 knockout mice were purchased from The Jackson Laboratory (Shank3Δ13-16, Stock No: 017688; Shank3Δ4-9, Stock No: 017890; jax.org). The brain-specific HCN2 knockout mice were generated by crossing the nestin-Cre mice (B6.Cg-Tg(Nes-Cre)1Kln/J; Stock No: 003771; jax.org) with Floxed-HCN2 mice (exons 3-4 floxed; kindly provided by Dr. Peter McNaughton from King's College, London).

Immunoblotting

Crude whole cell lysates were made of mouse brains from mice with comparable age groups. Brains were dissected and briefly rinsed in ice cold PBS. The brain was placed in a pre-chilled glass grinder with 1ml of ice cold lysis buffer (pH 7.35) composed of 150mM NaCl, 20mM Tris-HCL, 1% Triton-X, 0.1% SDS, 1mM each of EDTA and EGTA, 2mM PMSF, and 40µl of a Pierce Protease Inhibitor Tablet dissolved in 2x PBS. Each sample was homogenized by 20-25 strokes while on ice. After a brief incubation period, samples were transferred to Eppendorf tubes, sonicated for 15 secs each, and subjected to centrifugation to remove cellular debris. Lysates were then mixed with sample buffer containing 2-mercaptoethanol, boiled and centrifuged for 10 min each, and then loaded in to 10% SDS-polyacrylamide gels. Gels were transferred at 4°C to polyvinylidene difluoride membranes, and blots were subsequently washed two times in TBS-T. Blots were blocked in TBS-T containing 4% dry, non-fat milk, 1% goat serum, and 0.1% sodium azide for one hour at room temperature and then incubated with primary antibodies overnight at 4°C in the same blocking solution as described above (anti-HCN1 (1: 300), mouse anti-HCN2 (1: 1000), and rat anti-HCN4 (1: 2000); Novus Biologicals). The relative amount of β-actin was used as loading control (beta actin loading control (1: 1,000); Thermo Fisher Scientific). Blots were extensively washed three times with TBS-T and then incubated for one hour at room temperature with horseradish peroxidase conjugated secondary antibody at a dilution of 1: 20,000 in the same blocking solution. Blots were washed three times with TBS-T and then treated with ECL detection reagents (GE Healthcare and Thermo Scientific West Femto Maximum Sensitivity substrate at a ratio of 4:1, respectively).

3 Results

3.1 Yeast two-hybrid investigation of SHANK3 and HCN interactions

The yeast two-hybridization assay is a useful genetic tool used to detect protein-protein interactions. The strength of this system is its capability to provide a systematic survey of protein partners involved in interactions. Therefore, we used the Matchmaker™ Yeast two-hybridization system (Clontech Laboratories Inc.) to test for potential interactions between SHANK3 and HCN channels. Initially, we inserted five cDNA constructs of SHANK3 into pGBKT7 plasmids and used them as bait. The library plasmid (the prey) contained various cDNA fragments of the N- and C- termini of HCN1 and HCN2. We co-transformed various combinations of bait and prey plasmids into AH109 yeast and assayed for interactions by observing growth on Trp-/Leu-/His-depleted agar plates. Although we observed no colony growth from transformations containing pGBKT7_SHANK3-1, pGBKT7_SHANK3-3, and pGBKT7_SHANK3-5, we did observe a continuing pattern in which the bait plasmids pGBKT7_SHANK3-2 and pGBKT7_SHANK3-4 always generated positive results when they were co-transformed with any prey plasmid (Sup. Fig. 1).

This suggested that 1) either the PDZ or SH3 domains within the pGBKT7_SHANK3-2 plasmid or a pro-rich segment within the pGBKT7_SHANK3-4 plasmid a broadly interacts with the termini of HCN channels, or 2) that autoactivation of the yeast two-hybridization system by SHANK3 fragments may be occurring. Therefore, we created individual cDNA constructs for the PDZ and SH3 domains by separately cloning them into pGBKT7 plasmids. We found that the PDZ domain specifically was

responsible for all of the false-positive results we observed when originally co-expressing the pGBKT7_SHANK3-2 plasmid with pGADT7 plasmids containing HCN constructs (Sup. Fig. 2). To test for autoactivation, we co-transformed pGBKT7_SHANK3-2, pGBKT7_SHANK3-4, and pGBKT7_SHANK3-PDZ with empty pGADT7 plasmids. To our surprise, all three of these bait plasmids containing SHANK3 domains were able to autoactivate the system (Fig. 3). However, when we co-transformed pGBKT7_SHANK3-SH3 with HCN prey plasmids, we observed only one interaction from the pGBKT7_SHANK3-SH3 bait plasmid, which was with the pGADT7_m1-N plasmid (Fig. 4) and most likely the only positive hit.

To combat the issue of autoactivation, we swapped the cDNAs of PDZ and pro-rich domains from the pGBKT7 plasmid them into pGADT7 plasmids to create pGADT7_SHANK3-PDZ and pGADT7_SHANK3-Pro-rich. Likewise, we swapped the cDNAs of the CNBD and ext-C segments of the mHCN2 C-terminus from the pGADT7 plasmid to the pGBKT7 plasmid to create pGBKT7_m2-CNBD and pGBKT7_m2-ext-C. We then co-transformed pGADT7_SHANK3-PDZ and pGADT7_SHANK3-Pro-rich with pGBKT7_m2-CNBD and pGBKT7_m2-ext-C. We also lessened the stringency of the assay by chaning from quadruple dropout to triple drop out SD agar plates under the presumption that the interaction between SHANK3 and HCN2 may be transient. Under this condition, we did not observe any autoactivation, nor did we observe any interactions between the bait and prey plasmids (Fig. 5).

With the idea in mind that the interaction between SHANK3 and HCN may be transient, we decided to lessen the stringency and assay the original pGBKT7_SHANK3-1, pGBKT7_SHANK3-3, and pGBKT7_SHANK3-5 again. We co-

transformed each of these bait plasmids with the prey plasmids containing the cDNA of CNBD and Ext-C for both mHCN1 and mHCN2. Surprisingly, we observed positive results for all of these co-transformations accept for pGKT7_SHANK3-3 + pGADT7_m2-CNBD and pGBKT7_SHANK3-5 + pGADT7_m2-ext-C (Sup. Fig. 3). We again suspected the issue of autoactivation and so we co transformed pGBKT7_SHANK3-1, pGBKT7_SHANK3-3, and pGBKT7_SHANK3-5 each with an empty pGADT7 plasmid. We found that the bait plasmids pGBKT7_SHANK3-3 and pGBKT7_SHANK3-5 also have the ability to autoactivate the yeast two-hybrid system (Fig. 6).

Given that the bait plasmid pGBKT7_SHANK3-1 did not appear to autoactivate the yeast two-hybrid system, we co-transformed pGBKT7_SHANK3-1 with the following prey plasmids: pGADT7_m1-N, pGADT7_m2-N, pGADT7_m1-CNBD, pGADT7_m2-CNBD, pGADT7_m1-ext-C, and pGADT7_m2 ext-C. We also lessened stringency by performing the assay on triple dropout media. To our surprise again, we observed growth for all of these co-transformations (Sup. Fig 4). We decided to simultaneously test for auto activation and potential interactions between the pGBKT7_SHANK3-1 plasmid and the same six HCN-segment containing prey plasmids by performing drop test analysis. As shown in figure 7, the co-transformation of pGBKT7_SHANK3-1 with an empty pGADT7 plasmid resulted in the growth of colonies up to 10^{-3} dilutions. Indeed, unintentional variations between experimental conditions may account for the contrasting results of pGBKT7_SHANK3-1 bait plasmids.

Finally, we performed the same analysis as shown in Sup. Fig. 4, accept this time we used quadruple dropout media (Fig. 8). Interestingly, under these conditions, colony growth was only observed from co-transformations of pGBKT7_SHANK3-1 with

either pGADT7_m1-CNBD, pGADT7_m2-CNBD, or pGADT7_m2-ext-C. One possibility is that, although the bait plasmid pGBKT7_SHANK3-1 may be able to autoactivate the yeast two-hybrid system and give positive results on triple dropout media, its potential interaction with HCN C-terminal domains may augment the interaction in the yeast two-hybrid system and allow for colony growth on the highly stringent quadruple dropout media.

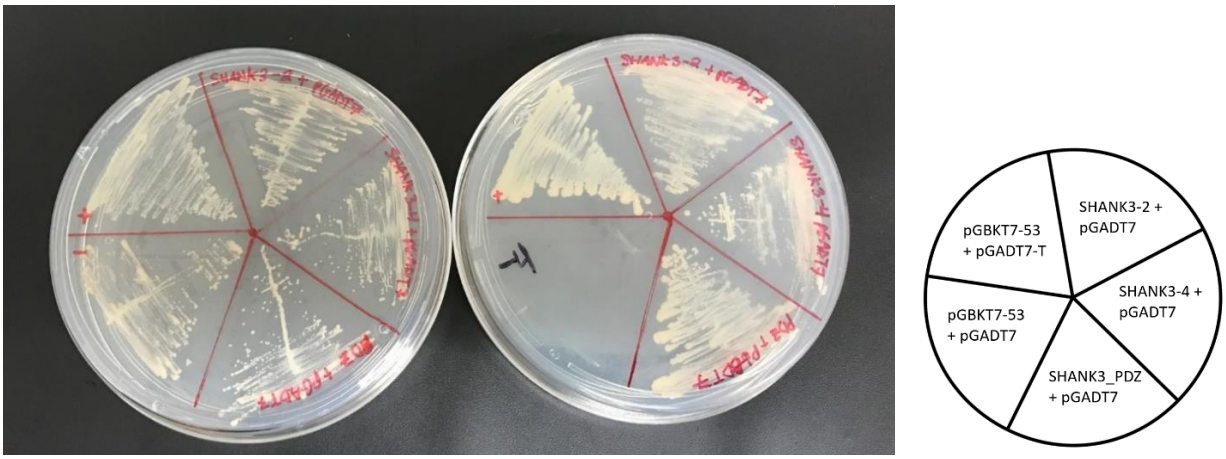

Figure 3. The PDZ and Pro-rich domains of SHANK3 can autoactivate the Matchmaker™ yeast two-hybrid system. pGBKT7_SHANK3-2, pGBKT7_SHANK3-4, and pGBKT7_PDZ were each co-transformed with empty pGADT7 plasmids and plated on depleted Trp-/Leu- SD media agar plates (not shown) to select for successful transformations. Single colonies from the control plates were picked and streaked onto SD depleted Trp-/Leu- and Trp-/Leu-/His-/Ade agar plates. Left: control plate with depleted Trp-/Lue- SD media selecting for successful transformation. Right: Assay plate with depleted Trp-/Leu-/His-/Ade- SD media selecting for protein-protein interactions.

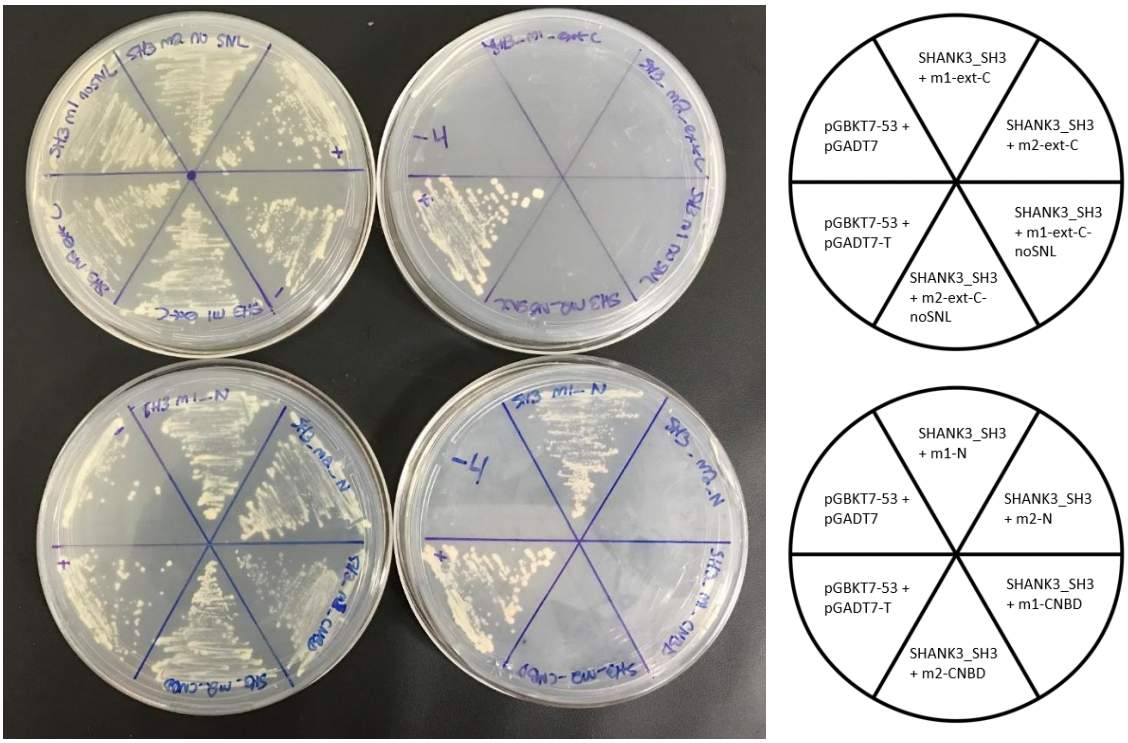

Figure 4: The SH3 domain does not autoactivate the Matchmaker Yeast two hybrid system. pGBKT7_SH3 was co-transformed with pGADT7_m1-N; m2-N; m1-CNBD; m2-CNBD; m1-ext-C; m2-ext-C; m1-ext-C_noSNL; and m2-ext-C_noSNL) and plated on Trp-/Lue- SD agar plates (not shown) to select for successful transformations. Single colonies from the control plates were picked and streaked onto depleted Trp-/Leu- and depleted Trp-/Leu-/His-/Ade- SD agar plates. Top and bottom left: control plates with depleted Trp-/Lue- SD media selecting for successful transformation. Top and bottom right: Assay plates with depleted Trp-/Leu-/His-/Ade- SD media selecting for protein-protein interactions.

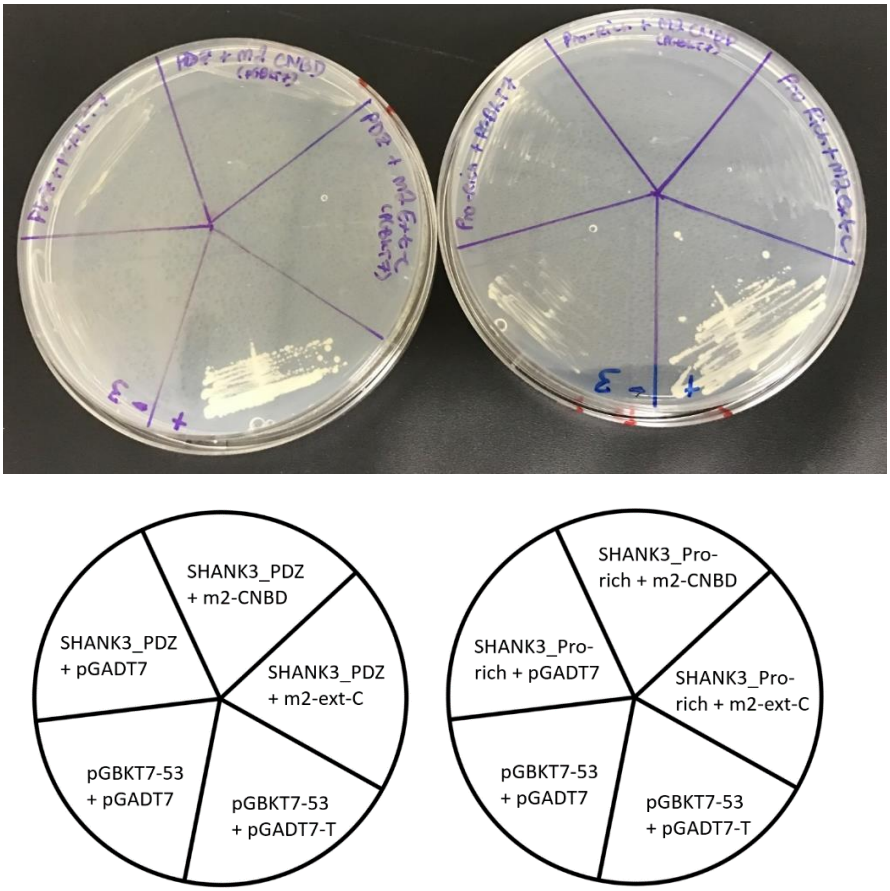

Figure 5: Switching the PDZ and Pro-rich domains from pGBKT7 into pGADT7 does not autoactivate the Matchmaker yeast two-hybrid system. pGADT7_PDZ was co transformed into AH109 with an empty pGBKT7 plasmid, pGBKT7_m2-CNBD, and pGBKT7_m2-ext-C and plated on depleted Trp-/Leu- SD media agar plates (not shown) to select for successful transformations. Single colonies from the control plates were picked and streaked onto SD depleted Trp-/Leu-/His- agar plates. Left: Assay plate with depleted Trp-/Leu-/His- SD media selecting for protein-protein interactions. Right: assay plate with depleted Trp-/Leu-/His- SD media selecting for protein-protein interactions. Note that the stringency was lowered by switching from quadruple dropout plates to triple dropout plates.

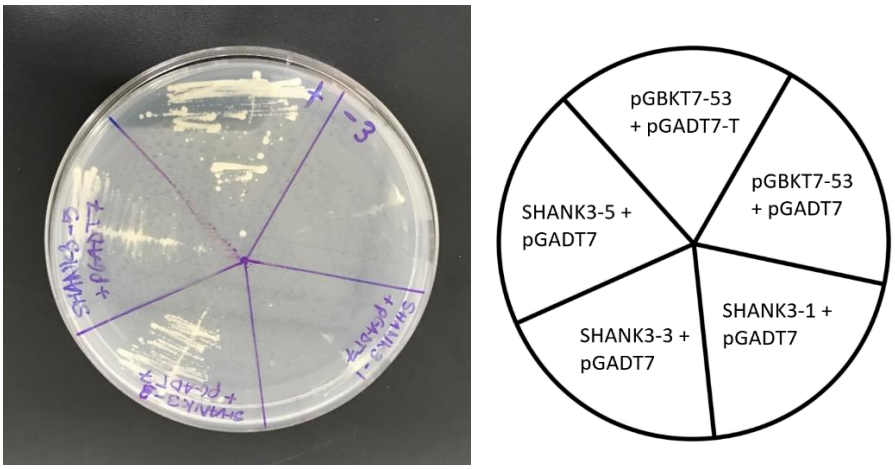

Figure 6. pGBKT7 plasmids containing Pro-rich and SAM domains can also activate the Matchmaker yeast two-hybrid system. pGBKT7_(SHANK3-1; SHANK3-3; and SHANK3-5) were each transformed with empty pGADT7 vectors into AH109 and grown on depleted Trp-/Leu- SD media agar plates (not shown) to select for successful transformations. Single colonies from the control plates were picked and streaked onto SD depleted Trp-/Leu-/His- agar plates to test for autoactivation.

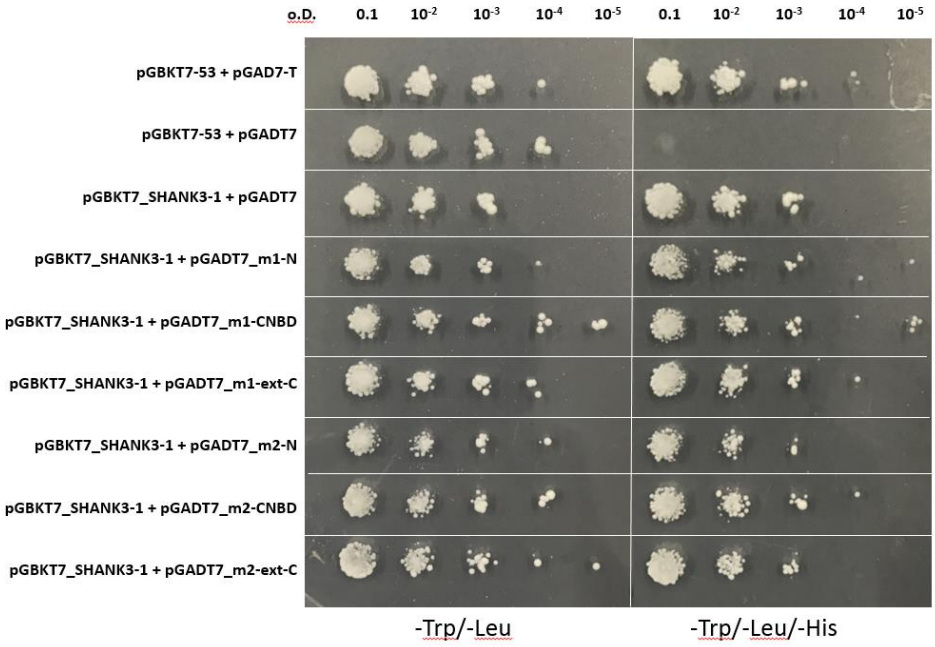

Figure 7: Drop test analysis of pGBKT7_SHANK3-1 reveals autoactivation.
pGBKT7_SHANK3-1 was co-transformed with each pGADT7_(m1-N; m2-N; m1-CNBD; m2-CNBD; m1-ext-C; and m2-ext-C) plasmid into AH109 and grown on depleted Trp-/Leu- SD agar plates. Individual colonies were selected and grown in depleted Trp-/Leu- SD media until the optical density (o.D.) of each sample was measure to 0.1. Samples were serial diluted to 10^{-1}, 10^{-2}, 10^{-3}, 10^{-4} and, 10^{-5} and then plated onto Trp-/Leu-(left) and Trp-/Leu-/His- (right) agar plates as seen above.

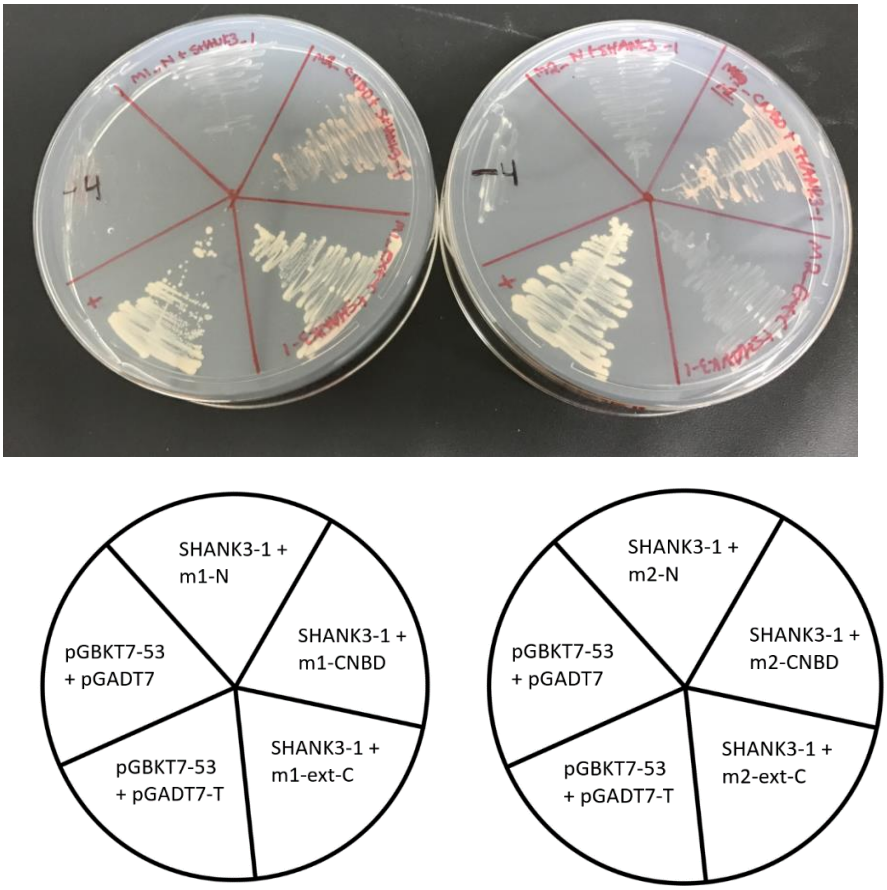

Figure 8: Less autoactivation of the Matchmaker yeast two-hybrid system via pGBKT7_SHANK3-1 under more stringent conditions. pGBKT7_SHANK3-1 was co-transformed with pGADT7_(m1-N; m2-N; m1-CNBD; m2-CNBD; m1-ext-C; and m2-ext-C) into AH109 and plated on depleted Trp-/Leu- SD agar plates (not shown) to select for successful transformations. Single colonies from the control plates were picked and streaked onto SD depleted Trp-/Leu-/His-/Ade- agar plates. Left: Assay plate with depleted Trp-/Leu-/His-/Ade- SD media selecting for protein-protein interactions. Right: assay plate with depleted Trp-/Leu-/His-/Ade- SD media selecting for protein-protein interactions. Note that the stringency was increased by switching from triple dropout plates to quadruple dropout plates.

3.2 Immunoblotting of HCN channels in SHANK3 deficient mice

As discussed above, SHANK3 haploinsufficiency can impair I_h currents, and an interaction between the ANK domain of SHANK3 and HCN channels has been revealed by protein pulldown assays (Yi et al., 2016). Our lab has also characterized the relationship between SHANK3 and HCN channels in thalamocortical neurons (not yet published). We have found that how SHANK3 deficiency causes I_h impairment is based on the cohort of Shank3 isoforms being deleted from the genome, and, more specifically, the design of the strategy to generate Shank3 knockout mouse models. As shown in figure 9 (image and data courtesy of Zhu Mengye; not yet published), I_h currents are impaired in the ventrobasal (VB) neurons of Shank3$^{\Delta 13\text{-}16}$ mice, but not from Shank3$^{\Delta 4\text{-}9}$ VB neurons. One likely explanation for this observation is that Shank3$^{\Delta 4\text{-}9}$ mice still express Shank3c, a major Shank3 isoform, while Shank3$^{\Delta 13\text{-}16}$ mice lose most of the isoform cohort (Fig. 10).

In order to substantiate the findings from the electrophysiology recordings, we decided to compare the levels of HCN channel proteins in whole brain lysates from WT, mutant Shank3$^{\Delta 13\text{-}16}$, and mutant Shank3$^{\Delta 4\text{-}9}$ mice using western blot analysis (Fig. 11). For negative control, we generated a brain-specific HCN2 knockout mouse model by crossing floxed-HCN2 (Emery et al., 2011) with Nestin-Cre mice, which we have termed HCN2$^{\Delta 2\text{-}3}$. Accordingly, the HCN2 band matching the molecular weight (~95 kDa) is absent in the HCN2$^{\Delta 2\text{-}3}$-/- lane (Fig 11a). Surprisingly, we observed almost a total loss of HCN2 expression in Shank3$^{\Delta 13\text{-}16}$-/- mice (Fig. 11b, lane 3) while Shank3$^{\Delta 4\text{-}9}$-/- mice showed no obvious loss of expression. Therefore, these results agree well with the electrophysiological recordings shown above (Fig 9). Next, we decided to investigate

whether the loss of SHANK3 would have similar effects on the expression of other members in the HCN channel family. Unexpectedly, we also observed an increase of HCN4 expression in HCN2$^{\Delta 2\text{-}3}$ +/- and HCN2$^{\Delta 2\text{-}3}$ -/- mice (Fig 12). Surprisingly, the expression of HCN4, but not HCN1, was increased in both HCN2$^{\Delta 2\text{-}3}$ and Shank3$^{\Delta 13\text{-}16}$ mice in comparison to the HCN4 expression in their WT littermates (Fig. 12). The expression of HCN4 was not altered in Shank3$^{\Delta 4\text{-}9}$ mice (data not shown).

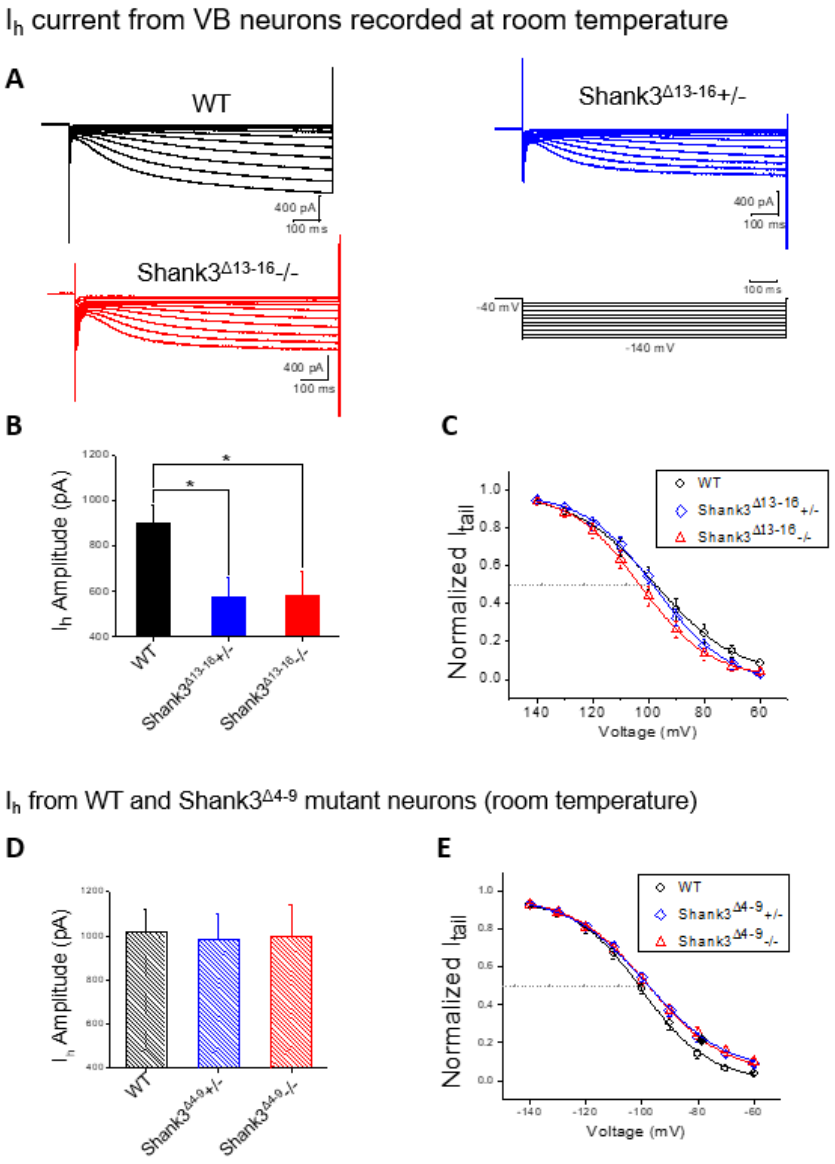

Fig. 9 The Ih current from Shank3$^{\Delta 13-16}$, but not from Shank3$^{\Delta 4-9}$ VB neurons, exhibits decreased current amplitude (all recordings were collected at room temperature). A. Representative Ih current traces recorded from VB neurons of WT (black), Shank3Δ13-16 +/- (blue), and Shank3Δ13-16 -/- (red) mice. Ih was activated by a series of hyperpolarizing voltage steps (bottom, right). B. Summary graphs of the Ih current amplitude measured at -120 mV of VB neurons from WT (black), Shank3Δ13-16 +/- (blue), and Shank3Δ13-16 -/- (red) mice (left) or WT (black), Shank3Δ4-9 +/- (blue), and Shank3Δ4-9 -/- (red) mice (right). C. Normalized tail current amplitudes (Itail) were plotted against voltage steps and fit with the Boltzmann equation. V1/2 values (mV): -97.8 ± 0.3 (WT); -97.6 ± 0.5 (Shank3Δ13-16+/-); -103.0 ± 0.3 (Shank3Δ13-16-/-). D. Summary graphs of the Ih current amplitude measured at -120 mV of VB neurons from WT (black), Shank3Δ4-9 +/- (blue), and Shank3Δ4-9 -/- (red) mice (right). E. Normalized tail current amplitudes (Itail) were plotted against voltage steps and fit with the Boltzmann equation. V1/2 values (mV): -100.0 ± 0.5 (WT); 97.8 ± 0.2 (Shank3Δ4-9+/-); -98.3 ± 0.4 (Shank3Δ4-9-/-). Image and data kindly provided by the courtesy of Mengye Zhu.

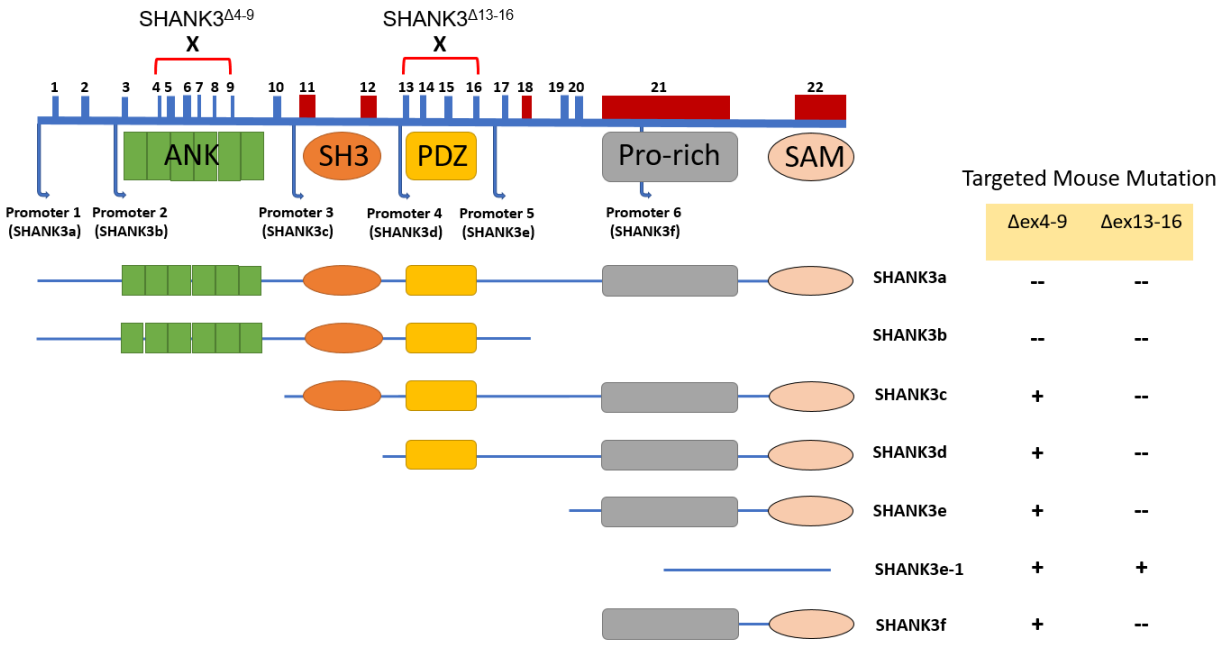

Figure 10. SHANK3$^{\Delta 13\text{-}16}$ mice lack most of the major isoforms. Cartoon representation showing differences between two different mouse models of autism. Loss of exons 4-9 in SHANK3$^{\Delta 4\text{-}9}$ mice results in the forfeiture of full length SHANK3 (SHANK3a) and SHANK3b. Loss of exons 13-16 in SHANK3$^{\Delta 13\text{-}16}$ mice results in the loss of all major SHANK3 isoforms. For example, SHANK3$^{\Delta 13\text{-}16}$ mice lack any SHANK3 isoform that contains ANK, SH3, and PDZ domains while SHANK3$^{\Delta 4\text{-}9}$ mice only lack isoforms containing ANK domains. A "+" indicates that the isoform is expressed in the mutant model while a "—" indicates the isoform is absent in the respective mouse model. It should be noted that although these are the known isoforms of SHANK3, this is not an exhaustive list and it is likely that other isoforms of SHANK3 have yet to be elucidated. Image adapted from (Wang et al., 2014b).

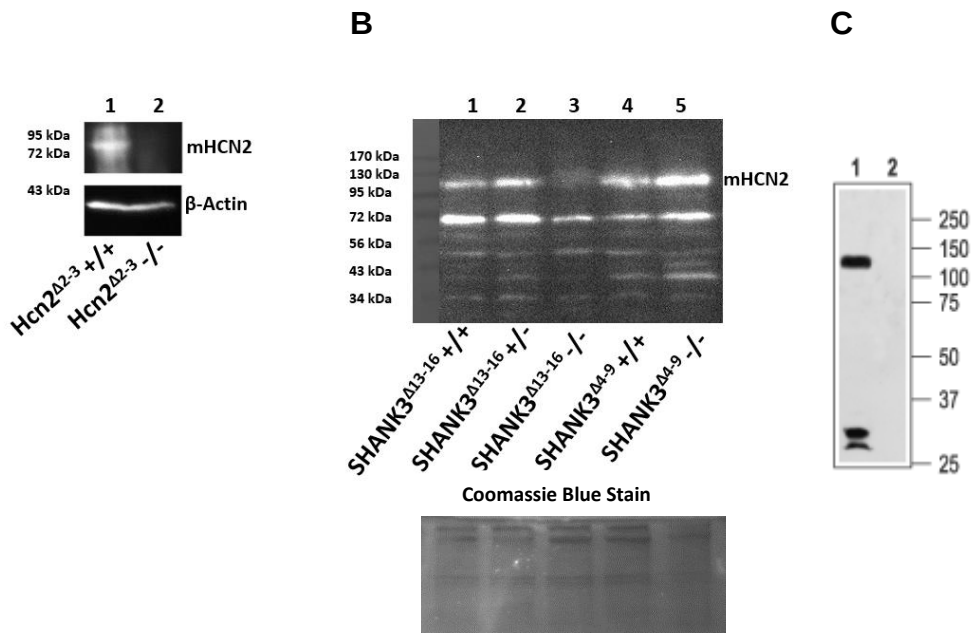

Figure 11. HCN2 expression is lost in Shank3$^{\Delta 13-16}$ -/- mice but not Shank3$^{\Delta 4-9}$ -/- mice. Proteins were isolated from whole brain lysates from mice of comparable age groups. Western blot (IB) analysis was performed on Hcn2$^{\Delta 2-3}$ **+/+** mice as a positive control and Hcn2$^{\Delta 2-3}$ **-/-** mice as a negative control (A) using a polyclonal anti-HCN2 antibody from UC Davis. (B) IB analysis was done on Shank3Δ13-16 and Shank3Δ4-9 mice using a monoclonal anti-HCN2 antibody from UC Alomone. As demonstrated in lane 3, there is only a very faint signal for HCN2 in Shank3Δ13-16 -/- mice. In lane 5, however, a band is present at the correct kDa showing that HCN2 is expressed in Shank3Δ4-9 -/- mice. We used β-Actin as a loading control in (A) and Coomassie blue stained gel as a loading control for (B). For reference, a representative western blot of HCN2 from Alomone labs is included (C).

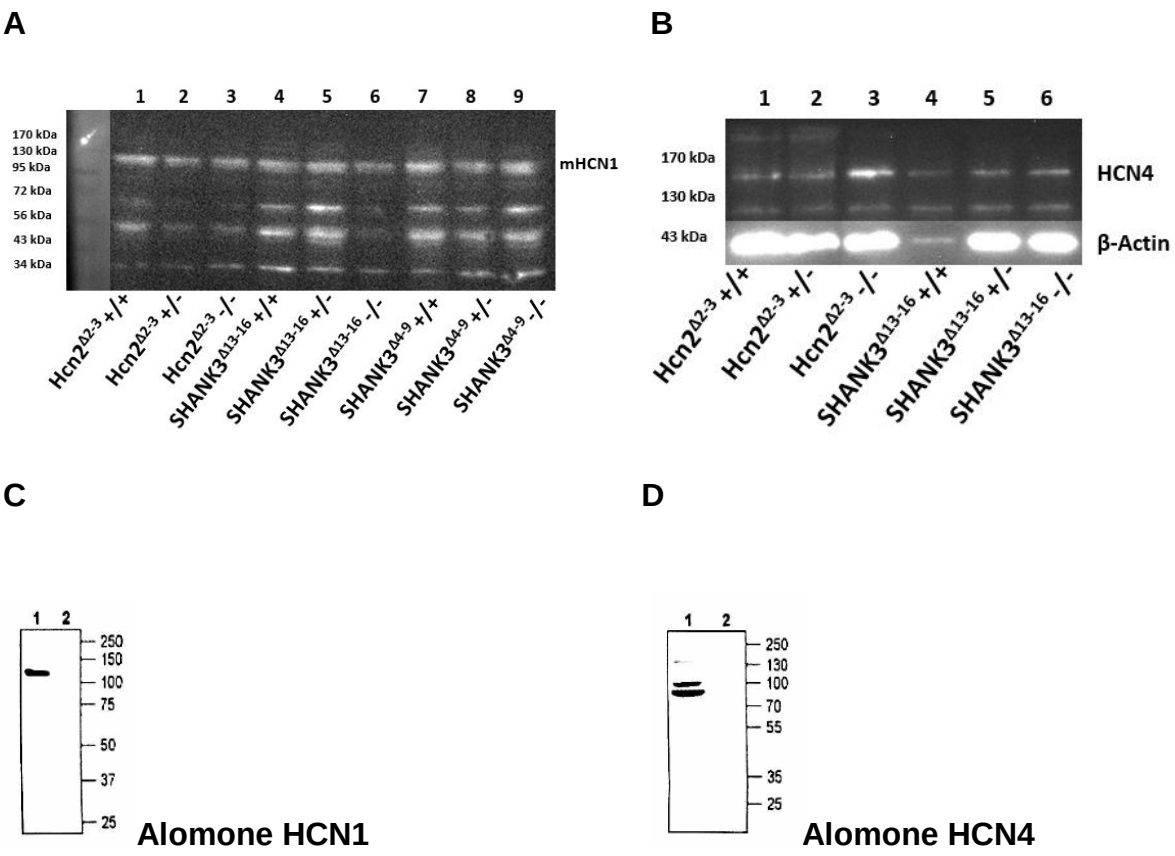

Figure 12. HCN4 expression, but not HCN1 expression increases in Shank3$^{\Delta 13\text{-}16}$ -/- mice and in HCN2$^{\Delta 2\text{-}3}$ mutant mice. Proteins were isolated from whole brain lysates from mice of comparable age groups. Western blot (IB) analysis was performed on Hcn2$^{\Delta 2\text{-}3}$, Shank3Δ13-16, and Shank3Δ4-9 mice using a polyclonal anti-HCN1 and anti-HCN4 antibodies from Alomone. (A) IB results of anti-HCN1. No drastic change in the expression of HCN1 is visibly apparent in any of the three mouse models analyzed. (B) IB results of anti-HCN4. Increased HCN4 expression can be seen in lanes 2, 3, 5 and 6, corresponding to HCN2$^{\Delta 2\text{-}3}$ +/-, HCN2$^{\Delta 2\text{-}3}$ -/-, Shank3$^{\Delta 13\text{-}16}$ +/- and Shank3$^{\Delta 13\text{-}16}$ -/- mice. For reference, representative western blots of HCN1 and HCN4 from Alomone labs are included (C & D).

4 Discussion

In this study, I tried to combine both yeast genetics (yeast-two hybridization) and protein biochemistry (Western Blotting) to tackle the Shank3 - HCN interaction. For the Y2H, I learned basic molecular cloning techniques and successfully cloned cDNA constructs of Shank3 or HCN into the corresponding vectors. Moreover, I grasped the basics of yeast genetics and successfully reproduced the positive and negative controls by using amino acid-omission SD media. Although our preliminary results are promising, they are also affected by the issue of autoactivation. Extensive discussions regarding the potential solutions are provided below. For the immunoblotting, I learned basic protein biochemistry techniques and gained substantial understanding about monoclonal and polyclonal antibodies. Importantly, I took advantage of the three different lines of knockout mouse models available in the lab and obtained convincing and exciting WB results. First, we confirmed the quality of the anti-HCN2 antibody by using the $HCN2^{\Delta 2\text{-}3}$-/- sample. Secondly, we show that the Shank3 deficiency has a specific impact on the expression of HCN2 but not of HCN1 or HCN4. Discussions are also provided below regarding this particular and intriguing observation.

4.1 Discussion on Yeast Two-Hybridization

This issue of autoactivation was a blight on our efforts. There are few other authors who have reported issues with autoactivation when using PDZ domains in a yeast two-hybrid system (Gisler et al., 2003). Nonetheless, we were presented with autoactivation from nearly every transformation of pGBKT7 plasmid containing SHANK

cDNA fragments. It is typically conventional to fuse the bait cDNA with the DNA binding domain (DBD) since the interaction between the DBD and the upstream activation sequence (UAS) is more stringent. Indeed, we used SHANK3 fragments as our bait. However, a small percentage of transcription initiation can be attributed to latent activation of a transcription factor from proteins, and this value increases with the random generation of cDNA fragments (Van Criekinge and Beyaert, 1999).

The fact that our cDNAs were fragments only encompassed poorly defined regions of SHANK3 domains and not strictly generated to suitably imitate the precise molecular structure SHANK3 protein domains may have attributed to these false positives. Therefore, in going forward with this genetic approach it may be useful to better define the cDNA constructs such that only the cDNA relevant to the specific domain is fused to the DBD. Nonetheless, after isolation of the SHANK3 PDZ domain and subsequent cloning into the pGBKT7 plasmid, we still observed autoactivation (Fig. 1). When we also isolated the SH3 domain, however, we did not observe autoactivation (Fig. 2). We observed a positive result from the co-transformation of pGBKT7_SHANK3-SH3 with pGADT7_m1-N. Given the stringency of the assay in which this test was performed (-Trp/-Leu/-His/-Ade depleted SD media) it is tempting to interpret this is a potential positive interaction. However, this should be interpreted with caution as the pGADT7_m1-N library plasmid was never assayed for autoactivation (i.e. co-transformation with an empty pGBKT7 plasmid).

The PDZ domain plays a critical role in the organization of proteins in the PSD, and the localization of this domain into the nucleus may cause undesirable effects in such an artificial system, especially considering that it is bound to the DBD when placed

into bait plasmids. Once we swapped the PDZ domain into the pGADT7 library vector, however, we no longer observed any false-positive growth on our assay plates (Fig. 3). Because the pGBKT7_SHANK3-4 (pro-rich containing fragment) also showed autoactivation, we cloned it into pGADT7 library plasmids to see if autoactivation would still occur. Indeed, there was no autoactivation (Fig. 3), suggesting that, at least for these two fragments, their cloning into pGADT7 library plasmids in the Matchmaker® Yeast Two-Hybrid System is critical to avoid autoactivation. Moreover, it may prove fruitful to clone the HCN cDNA fragments into pGBKT7 plasmids and use them as bait against a SHANK3 library cloned into the pGADT7 plasmid.

Another potential issue with this assay may be a low-level expression of histidine. Although AH109 yeast is engineered to only express the HIS3 gene upon activation of the GAL4 promoter, low level expression and thus background growth on media lacking His may still be occurring. Since 3-AT is competitive inhibitor of the HIS3 protein, optimizing the concentration of this compound within the media may also eliminate unwanted growth (Durfee et al., 1993; Fields, 1993). Indeed, the use of 3-AT on -Trp/-Leu/-His media and co-transformation of pGBKT7_SHANK3-1 with an empty pGADT7 vector may be sufficient to prevent colony growth, as seen in our autoactivation drop test analysis in figure 5.

Another advantage of the AH109 yeast strain is the ADE2 reporter gene (James et al., 1996). In this strain, the non-essential ADE2 gene has a null mutation which results in the accumulation of an intermediate product during the biosynthesis of adenine. Consequently, AH109 colonies present as pink or red in color unless adenine is present in the SD media. However, AH109 yeast have a functional ADE2 gene under

the control of a GAL4 promoter, implying that any protein-protein interactions from the Matchmaker® plasmids will express ADE2 and present as white colonies on adenine deficient SD media. Although we found that under moderately stringent conditions (-Trp/-Leu/-His SD agar) that pGBKT7_SHANK3-1 (ANK domain containing) could autoactivate the yeast two-hybrid system, we observed no colony growth on highly stringent media (-Trp/-Leu/-His/-Ade) between pGBKT7_SHANK3-1 with pGADT7_m1-N, pGADT7_m2-N, or pGADT7_m2-ext-C. Instead, we observed red colonies from the co-transformation of pGBKT7_SHANK3-1 with pGADT7_m1-CNBD and pGADT7_m2-CNBD. In comparison to the positive control colonies, the colonies from the co-transformation of pGBKT7_SHANK3-1 with the m1- and m2-CNBD containing pGADT7 plasmids were pink in color, indicating the ADE2 reporter gene was not expressed and thus may be a false positive. Interestingly, we observed white colonies from the co-transformation of pGBKT7_SHANK3-1 with pGADT7_m1-ext-C (Fig. 6), which prompts the speculation that this is a promising result for a number of reasons. First, while the issue of autoactivation in figure 5 cannot be ruled out, the possibility that residual His expression allowed for growth during that assay cannot be ruled out either. Second, although autoactivation or residual His expression might be possibilities on -Trp/-Leu/-His depleted SD media, there are both positive and negative results between pGBKT7_SHANK3-1 and various HCN containing library plasmids, as seen on the -Trp/-Leu/-His/-Ade depleted SD media in figure 6. This suggests that potential interactions between SHANK3 and mHCN2 may augment the Matchmaker® system under these stringent conditions. Another reason is that the colonies resulting from the co-transformations of pGBKT7_SHANK3-1 and pGADT7_m1-ext-C were white in color,

implying that the ADE2 reporter gene was expressed. Finally, it has recently been shown via coimmunoprecipitation assays that the ANK repeat of SHANK3 specifically interacts with HCN channels (Yi et al., 2016).

Taken together, the investigation between SHANK3 and HCN via the yeast two-hybrid assay may still serve as a fruitful method to characterize the physical interactions between these two proteins. Future experiments should utilize the LacZ reporter gene under control of the GAL4 promoter in AH109 yeast. This would further reduce the level of false positives and also allow for a quantitative analysis of the binding strength. More radical approaches may also be considered as well. For example, it was shown that, instead of fusing the C-terminus of the DBD to the N-terminus of the protein of interest, inverting the complex such that the N-terminus of the protein of interest is 'free' not only proved viable but increased the binding efficiency between the proteins of interest (Béranger et al., 1997). Indeed, exposing the N-terminal segments of SHANK3 bait may reveal missed interactions, as well as inhibit the issue of auto activation.

4.2 Discussion on Immunoblotting

A major finding in this study is that the differences between the targeted mutations in mouse models of autism have opposing effects on HCN channel expression. We showed that in Shank3$^{\Delta 13\text{-}16}$ -/- mice, the expression of HCN2 is significantly decreased. However, HCN2 expression is unaltered in Shank3$^{\Delta 4\text{-}9}$ -/- mice. These findings corroborate well with the electrophysiological studies our lab has done on VB neurons of Shank3$^{\Delta 13\text{-}16}$ -/- and Shank3$^{\Delta 4\text{-}9}$ -/- mice. Indeed, the significant

difference between these two mouse models is the expression of SHANK3 isoforms. In Shank3$^{\Delta 4\text{-}9}$ -/- mice, the only SHANK3 isoforms lost are SHANK3a and SHANK3b. In Shank3$^{\Delta 13\text{-}16}$ -/- mice, however, all major isoforms are lost. SHANK3a, SHANK3b, and SHANK3c all possess functional SH3 and PDZ domains. Therefore, it is tempting to speculate that in Shank3$^{\Delta 4\text{-}9}$ -/- mice, SHANK3c may be responsible for the mostly normal expression of HCN channels, thus explaining the difference in I_h currents and protein expression between the models we examined in this study. In fact, our lab has also shown that Shank3c alone is sufficient to increase the I_h current amplitude in *Xenopus* oocytes injected with cRNAs encoding HCN2 (not yet published). However, the fact that we did not observe any interactions between the PDZ or SH3 domain of SHANK3 with the N- or C-termini of HCN2 during our yeast two-hybrid investigation confounds this hypothesis. Nonetheless, SHANK3c and other isoforms may have a role in vesicular trafficking, ensuring the proper expression HCN channels. Indeed, loss of SHANK3 has shown to affect receptor trafficking of NMDA and AMPA (Jiang and Ehlers, 2013; Raynaud et al., 2013; Sarowar and Grabrucker, 2016).

Another unexpected finding in our preliminary study was that HCN4 expression appears to increase not only in HCN2$^{\Delta 2\text{-}3}$ mice, but also in SHANK3 $^{\Delta 13\text{-}16}$ mice. This observation warrants the question of whether or not the same pathways that induce increased HCN4 expression is similar between HCN2$^{\Delta 2\text{-}3}$ and SHANK3 $^{\Delta 13\text{-}16}$ mice. Although the primary amino acid sequences for all four HCN channel family members are highly similar in sequence, HCN2 and HCN4 share the highest homology and tend to form heteromers (Jackson et al., 2007). Although the activation constants for HCN2 and HCN4 are not comparable, with HCN4 being much slower to activate, they do share

high homology and many other biophysical characteristics (Table 1; Biel et al., 2009; Wang et al., 2001). The co-assembly of HCN2 and HCN4 to form heteromeric channels has been shown by multiple groups (Whitaker et al., 2007; Ye and Nerbonne, 2009; Zhang et al., 2009). One study showed that HCN2 and HCN4 show no preference in terms of homo- or heteromerization (Whitaker et al., 2007).The same study also demonstrated the co-assembly of HCN2 an HCN4 in rat thalamus. Therefore, it is tempting to speculate that in the absence of HCN2, HCN4 expression may increase to compensate for the loss of HCN2. Future experiments utilizing RT-qPCR to could verify this observation.

We did not observe any obvious changes of HCN1 expression across the three mouse models being analyzed. Therefore, of the three isoforms we analyzed (HCN1,2, and 4) in SHANK3 $^{\Delta 13\text{-}16}$ mice, it appears that the effect on neuronal physiology by impaired SHANK3 pathways may be carried downstream specifically by HCN2. In the thalamus, the expression of Shank3 and HCN2 predominates over those of Shank1,2 and HCN1,3,4, respectively (Sheng and Kim, 2002). Indeed, these expression profiles substantiate our labs work on SHANK3 and HCN2 in the VB neurons of mouse thalamus (not yet published). Taken together, these results support such a model that HCN2 channelopathy plays a key role in mediating the downstream detrimental effects induced by Shank3 deficiency.

4.3 Concluding Remarks

The Shank3 protein is of significant size, contains multiple highly conserved domains for mediating protein-protein interactions, and is known to interact with many different types of ion channels and receptors. We will continue to use biochemistry and physiology approaches to investigate the impacts on the function and expression of these cell surface proteins by Shank3. However, our biochemical assays and the electrophysiology characterization of neurons from three different HCN and Shank3 knockout mice, especially the similarities between HCN-/- and Shank3-/- neurons, suggests that impairments of HCN channel function play a dominant role in mediating the detrimental effects induced by Shank3 mutations.

List of References

Altomare, C., Terragni, B., Brioschi, C., Milanesi, R., Pagliuca, C., Viscomi, C., Moroni, A., Baruscotti, M., and DiFrancesco, D. (2003). Heteromeric HCN1–HCN4 channels: a comparison with native pacemaker channels from the rabbit sinoatrial node. J. Physiol. *549*, 347–359.

American Psychiatric Association (2013). Diagnostic and statistical manual of mental disorders (Washington, DC: American Psychiatric Publishing).

Atherton, J.F., Kitano, K., Baufreton, J., Fan, K., Wokosin, D., Tkatch, T., Shigemoto, R., Surmeier, D.J., and Bevan, M.D. (2010). Selective participation of somatodendritic HCN channels in inhibitory but not excitatory synaptic integration in neurons of the subthalamic nucleus. J. Neurosci. Off. J. Soc. Neurosci. *30*, 16025–16040.

Baruscotti, M., Bucchi, A., and Difrancesco, D. (2005). Physiology and pharmacology of the cardiac pacemaker (“funny”) current. Pharmacol. Ther. *107*, 59–79.

Baruscotti, M., Bottelli, G., Milanesi, R., DiFrancesco, J.C., and DiFrancesco, D. (2010). HCN-related channelopathies. Pflugers Arch. *460*, 405–415.

Bayliss, D.A., Viana, F., Bellingham, M.C., and Berger, A.J. (1994). Characteristics and postnatal development of a hyperpolarization-activated inward current in rat hypoglossal motoneurons in vitro. J. Neurophysiol. *71*, 119–128.

Bender, R.A., Soleymani, S.V., Brewster, A.L., Nguyen, S.T., Beck, H., Mathern, G.W., and Baram, T.Z. (2003). Enhanced expression of a specific hyperpolarization-activated cyclic nucleotide-gated cation channel (HCN) in surviving dentate gyrus granule cells of human and experimental epileptic hippocampus. J. Neurosci. Off. J. Soc. Neurosci. *23*, 6826–6836.

Béranger, F., Aresta, S., de Gunzburg, J., and Camonis, J. (1997). Getting more from the two-hybrid system: N-terminal fusions to LexA are efficient and sensitive baits for two-hybrid studies. Nucleic Acids Res. *25*, 2035–2036.

Berger, T., Larkum, M.E., and Lüscher, H.R. (2001). High I(h) channel density in the distal apical dendrite of layer V pyramidal cells increases bidirectional attenuation of EPSPs. J. Neurophysiol. *85*, 855–868.

Berkel, S., Marshall, C.R., Weiss, B., Howe, J., Roeth, R., Moog, U., Endris, V., Roberts, W., Szatmari, P., Pinto, D., et al. (2010). Mutations in the SHANK2 synaptic

scaffolding gene in autism spectrum disorder and mental retardation. Nat. Genet. *42*, 489–491.

Berkel, S., Tang, W., Treviño, M., Vogt, M., Obenhaus, H.A., Gass, P., Scherer, S.W., Sprengel, R., Schratt, G., and Rappold, G.A. (2012). Inherited and de novo SHANK2 variants associated with autism spectrum disorder impair neuronal morphogenesis and physiology. Hum. Mol. Genet. *21*, 344–357.

Biel, M., Schneider, A., and Wahl, C. (2002). Cardiac HCN Channels. Trends Cardiovasc. Med. *12*, 206–213.

Biel, M., Wahl-Schott, C., Michalakis, S., and Zong, X. (2009). Hyperpolarization-activated cation channels: from genes to function. Physiol. Rev. *89*, 847–885.

Bobker, D.H., and Williams, J.T. (1989). Serotonin augments the cationic current Ih in central neurons. Neuron *2*, 1535–1540.

Boccuto, L., Lauri, M., Sarasua, S.M., Skinner, C.D., Buccella, D., Dwivedi, A., Orteschi, D., Collins, J.S., Zollino, M., Visconti, P., et al. (2013). Prevalence of SHANK3 variants in patients with different subtypes of autism spectrum disorders. Eur. J. Hum. Genet. *21*, 310–316.

Böckers, T.M., Mameza, M.G., Kreutz, M.R., Bockmann, J., Weise, C., Buck, F., Richter, D., Gundelfinger, E.D., and Kreienkamp, H.-J. (2001). Synaptic Scaffolding Proteins in Rat Brain ANKYRIN REPEATS OF THE MULTIDOMAIN Shank PROTEIN FAMILY INTERACT WITH THE CYTOSKELETAL PROTEIN α-FODRIN. J. Biol. Chem. *276*, 40104–40112.

Boeckers, T.M., Kreutz, M.R., Winter, C., Zuschratter, W., Smalla, K.H., Sanmarti-Vila, L., Wex, H., Langnaese, K., Bockmann, J., Garner, C.C., et al. (1999a). Proline-rich synapse-associated protein-1/cortactin binding protein 1 (ProSAP1/CortBP1) is a PDZ-domain protein highly enriched in the postsynaptic density. J. Neurosci. Off. J. Soc. Neurosci. *19*, 6506–6518.

Boeckers, T.M., Winter, C., Smalla, K.-H., Kreutz, M.R., Bockmann, J., Seidenbecher, C., Garner, C.C., and Gundelfinger, E.D. (1999b). Proline-Rich Synapse-Associated Proteins ProSAP1 and ProSAP2 Interact with Synaptic Proteins of the SAPAP/GKAP Family. Biochem. Biophys. Res. Commun. *264*, 247–252.

Boeckers, T.M., Bockmann, J., Kreutz, M.R., and Gundelfinger, E.D. (2002). ProSAP/Shank proteins - a family of higher order organizing molecules of the postsynaptic density with an emerging role in human neurological disease. J. Neurochem. *81*, 903–910.

Bolton, P.F., Golding, J., Emond, A., and Steer, C.D. (2012). Autism spectrum disorder and autistic traits in the Avon Longitudinal Study of Parents and Children: precursors and early signs. J. Am. Acad. Child Adolesc. Psychiatry *51*, 249–260.e25.

Bonaglia, M.C., Giorda, R., Mani, E., Aceti, G., Anderlid, B.-M., Baroncini, A., Pramparo, T., and Zuffardi, O. (2006). Identification of a recurrent breakpoint within the *SHANK3* gene in the 22q13.3 deletion syndrome. J. Med. Genet. *43*, 822–828.

Boyle, C.A., Boulet, S., Schieve, L.A., Cohen, R.A., Blumberg, S.J., Yeargin-Allsopp, M., Visser, S., and Kogan, M.D. (2011). Trends in the Prevalence of Developmental Disabilities in US Children, 1997–2008. Pediatrics peds.2010-2989.

Bozdagi, O., Sakurai, T., Papapetrou, D., Wang, X., Dickstein, D.L., Takahashi, N., Kajiwara, Y., Yang, M., Katz, A.M., Scattoni, M.L., et al. (2010). Haploinsufficiency of the autism-associated Shank3 gene leads to deficits in synaptic function, social interaction, and social communication. Mol. Autism *1*, 15.

Brewster, A., Bender, R.A., Chen, Y., Dube, C., Eghbal-Ahmadi, M., and Baram, T.Z. (2002). Developmental Febrile Seizures Modulate Hippocampal Gene Expression of Hyperpolarization-Activated Channels in an Isoform- and Cell-Specific Manner. J. Neurosci. *22*, 4591–4599.

Brown, H.F., Difrancesco, D., and Noble, S.J. (1979a). How does adrenaline accelerate the heart? Nature *280*, 235–236.

Brown, H.F., DiFrancisco, D., and Noble, S.J. (1979b). Adrenaline action on rabbit sino-atrial node [proceedings]. J. Physiol. *290*, 31P–32P.

Carlson, G.C. (2012). Glutamate receptor dysfunction and drug targets across models of autism spectrum disorders. Pharmacol. Biochem. Behav. *100*, 850–854.

Chan, C.S., Glajch, K.E., Gertler, T.S., Guzman, J.N., Mercer, J.N., Lewis, A.S., Goldberg, A.B., Tkatch, T., Shigemoto, R., Fleming, S.M., et al. (2011). HCN Channelopathy in External Globus Pallidus Neurons in Models of Parkinson's Disease. Nat. Neurosci. *14*, 85–92.

Chaste, P., and Leboyer, M. (2012). Autism risk factors: genes, environment, and gene-environment interactions. Dialogues Clin. Neurosci. *14*, 281–292.

Chen, J., Mitcheson, J.S., Lin, M., and Sanguinetti, M.C. (2000). Functional roles of charged residues in the putative voltage sensor of the HCN2 pacemaker channel. J. Biol. Chem. *275*, 36465–36471.

Chen, S., Wang, J., and Siegelbaum, S.A. (2001). Properties of hyperpolarization-activated pacemaker current defined by coassembly of HCN1 and HCN2 subunits and basal modulation by cyclic nucleotide. J. Gen. Physiol. *117*, 491–504.

Christensen, D.L. (2016). Prevalence and Characteristics of Autism Spectrum Disorder Among Children Aged 8 Years — Autism and Developmental Disabilities Monitoring Network, 11 Sites, United States, 2012. MMWR Surveill. Summ. *65*.

Chung, W.K., Shin, M., Jaramillo, T.C., Leibel, R.L., LeDuc, C.A., Fischer, S.G., Tzilianos, E., Gheith, A.A., Lewis, A.S., and Chetkovich, D.M. (2009). Absence epilepsy in apathetic, a spontaneous mutant mouse lacking the h channel subunit, HCN2. Neurobiol. Dis. *33*, 499–508.

Constantino, J.N., Zhang, Y., Frazier, T., Abbacchi, A.M., and Law, P. (2010). Sibling recurrence and the genetic epidemiology of autism. Am. J. Psychiatry *167*, 1349–1356.

Craven, K.B., and Zagotta, W.N. (2006). CNG and HCN channels: two peas, one pod. Annu. Rev. Physiol. *68*, 375–401.

DiFrancesco, D. (1993). Pacemaker mechanisms in cardiac tissue. Annu. Rev. Physiol. *55*, 455–472.

DiFrancesco, D., and Tortora, P. (1991). Direct activation of cardiac pacemaker channels by intracellular cyclic AMP. Nature *351*, 145–147.

DiFrancesco, D., and Tromba, C. (1988a). Inhibition of the hyperpolarization-activated current (if) induced by acetylcholine in rabbit sino-atrial node myocytes. J. Physiol. *405*, 477–491.

DiFrancesco, D., and Tromba, C. (1988b). Muscarinic control of the hyperpolarization-activated current (if) in rabbit sino-atrial node myocytes. J. Physiol. *405*, 493–510.

DiFrancesco, D., Ducouret, P., and Robinson, R.B. (1989). Muscarinic modulation of cardiac rate at low acetylcholine concentrations. Science *243*, 669–671.

DiFrancesco, J.C., Barbuti, A., Milanesi, R., Coco, S., Bucchi, A., Bottelli, G., Ferrarese, C., Franceschetti, S., Terragni, B., Baruscotti, M., et al. (2011). Recessive loss-of-function mutation in the pacemaker HCN2 channel causing increased neuronal excitability in a patient with idiopathic generalized epilepsy. J. Neurosci. Off. J. Soc. Neurosci. *31*, 17327–17337.

DiGuiseppi, C., Hepburn, S., Davis, J.M., Fidler, D.J., Hartway, S., Lee, N.R., Miller, L., Ruttenber, M., and Robinson, C. (2010). Screening for autism spectrum disorders in children with Down syndrome: population prevalence and screening test characteristics. J. Dev. Behav. Pediatr. JDBP *31*, 181–191.

Doan, T.N., and Kunze, D.L. (1999). Contribution of the hyperpolarization-activated current to the resting membrane potential of rat nodose sensory neurons. J. Physiol. *514 (Pt 1)*, 125–138.

Doshi-Velez, F., Ge, Y., and Kohane, I. (2014). Comorbidity Clusters in Autism Spectrum Disorders: An Electronic Health Record Time-Series Analysis. Pediatrics *133*, e54–e63.

Dossi, R.C., Nuñez, A., and Steriade, M. (1992). Electrophysiology of a slow (0.5-4 Hz) intrinsic oscillation of cat thalamocortical neurones in vivo. J. Physiol. *447*, 215–234.

Dube, C., Chen, K., Eghbal-Ahmadi, M., Brunson, K., Soltesz, I., and Baram, T.Z. (2000). Prolonged febrile seizures in the immature rat model enhance hippocampal excitability long term. Ann. Neurol. *47*, 336–344.

Duffney, L.J., Wei, J., Cheng, J., Liu, W., Smith, K.R., Kittler, J.T., and Yan, Z. (2013). Shank3 Deficiency Induces NMDA Receptor Hypofunction via an Actin-Dependent Mechanism. J. Neurosci. *33*, 15767–15778.

Duffney, L.J., Zhong, P., Wei, J., Matas, E., Cheng, J., Qin, L., Ma, K., Dietz, D.M., Kajiwara, Y., Buxbaum, J.D., et al. (2015). Autism-like Deficits in Shank3-Deficient Mice Are Rescued by Targeting Actin Regulators. Cell Rep. *11*, 1400–1413.

Duman, R.S., and Nestler, E.J. (1999). Functional Roles for cAMP and cGMP.

Durand, C.M., Betancur, C., Boeckers, T.M., Bockmann, J., Chaste, P., Fauchereau, F., Nygren, G., Rastam, M., Gillberg, I.C., Anckarsäter, H., et al. (2007). Mutations in the gene encoding the synaptic scaffolding protein SHANK3 are associated with autism spectrum disorders. Nat. Genet. *39*, 25–27.

Durand, C.M., Perroy, J., Loll, F., Perrais, D., Fagni, L., Bourgeron, T., Montcouquiol, M., and Sans, N. (2012). SHANK3 mutations identified in autism lead to modification of dendritic spine morphology via an actin-dependent mechanism. Mol. Psychiatry *17*, 71–84.

Durfee, T., Becherer, K., Chen, P.L., Yeh, S.H., Yang, Y., Kilburn, A.E., Lee, W.H., and Elledge, S.J. (1993). The retinoblastoma protein associates with the protein phosphatase type 1 catalytic subunit. Genes Dev. *7*, 555–569.

Durkin, M.S., Maenner, M.J., Newschaffer, C.J., Lee, L.-C., Cunniff, C.M., Daniels, J.L., Kirby, R.S., Leavitt, L., Miller, L., Zahorodny, W., et al. (2008). Advanced parental age and the risk of autism spectrum disorder. Am. J. Epidemiol. *168*, 1268–1276.

Ehlers, M.D. (1999). Synapse structure: glutamate receptors connected by the shanks. Curr. Biol. CB *9*, R848-850.

Emery, E.C., Young, G.T., Berrocoso, E.M., Chen, L., and McNaughton, P.A. (2011). HCN2 Ion Channels Play a Central Role in Inflammatory and Neuropathic Pain. Science *333*, 1462–1466.

Fagerberg, L., Hallström, B.M., Oksvold, P., Kampf, C., Djureinovic, D., Odeberg, J., Habuka, M., Tahmasebpoor, S., Danielsson, A., Edlund, K., et al. (2014). Analysis of the human tissue-specific expression by genome-wide integration of transcriptomics and antibody-based proteomics. Mol. Cell. Proteomics MCP *13*, 397–406.

Fields, S. (1993). The Two-Hybrid System to Detect Protein-Protein Interactions. Methods *5*, 116–124.

Frazier, T.W., Georgiades, S., Bishop, S.L., and Hardan, A.Y. (2014). Behavioral and cognitive characteristics of females and males with autism in the Simons Simplex Collection. J. Am. Acad. Child Adolesc. Psychiatry *53*, 329-340.e1-3.

Fuccillo, M.V. (2016). Striatal Circuits as a Common Node for Autism Pathophysiology. Front. Neurosci. *10*.

Gauss, R., Seifert, R., and Kaupp, U.B. (1998). Molecular identification of a hyperpolarization-activated channel in sea urchin sperm. Nature *393*, 583–587.

Gauthier, J., Spiegelman, D., Piton, A., Lafrenière, R.G., Laurent, S., St-Onge, J., Lapointe, L., Hamdan, F.F., Cossette, P., Mottron, L., et al. (2009). Novel de novo SHANK3 mutation in autistic patients. Am. J. Med. Genet. Part B Neuropsychiatr. Genet. Off. Publ. Int. Soc. Psychiatr. Genet. *150B*, 421–424.

Gauthier, J., Champagne, N., Lafrenière, R.G., Xiong, L., Spiegelman, D., Brustein, E., Lapointe, M., Peng, H., Côté, M., Noreau, A., et al. (2010). De novo mutations in the gene encoding the synaptic scaffolding protein SHANK3 in patients ascertained for schizophrenia. Proc. Natl. Acad. Sci. U. S. A. *107*, 7863–7868.

Gilman, S.R., Iossifov, I., Levy, D., Ronemus, M., Wigler, M., and Vitkup, D. (2011). Rare De Novo Variants Associated with Autism Implicate a Large Functional Network of Genes Involved in Formation and Function of Synapses. Neuron *70*, 898–907.

Gisler, S.M., Pribanic, S., Bacic, D., Forrer, P., Gantenbein, A., Sabourin, L.A., Tsuji, A., Zhao, Z.-S., Manser, E., Biber, J., et al. (2003). PDZK1: I. A major scaffolder in brush borders of proximal tubular cells11See Editorial by Moe, p. 1916. Kidney Int. *64*, 1733–1745.

Good, C.H., Hoffman, A.F., Hoffer, B.J., Chefer, V.I., Shippenberg, T.S., Bäckman, C.M., Larsson, N.-G., Olson, L., Gellhaar, S., Galter, D., et al. (2011). Impaired nigrostriatal function precedes behavioral deficits in a genetic mitochondrial model of Parkinson's disease. FASEB J. Off. Publ. Fed. Am. Soc. Exp. Biol. *25*, 1333–1344.

Hallmayer, J., Cleveland, S., Torres, A., Phillips, J., Cohen, B., Torigoe, T., Miller, J., Fedele, A., Collins, J., Smith, K., et al. (2011). Genetic heritability and shared environmental factors among twin pairs with autism. Arch. Gen. Psychiatry *68*, 1095–1102.

Hasan, M.T., Hernández-González, S., Dogbevia, G., Treviño, M., Bertocchi, I., Gruart, A., and Delgado-García, J.M. (2013). Role of motor cortex NMDA receptors in learning-dependent synaptic plasticity of behaving mice. Nat. Commun. *4*, 2258.

Holtmann, M., Bölte, S., and Poustka, F. (2007). Autism spectrum disorders: sex differences in autistic behaviour domains and coexisting psychopathology. Dev. Med. Child Neurol. *49*, 361–366.

Huang, Z., Walker, M.C., and Shah, M.M. (2009). Loss of dendritic HCN1 subunits enhances cortical excitability and epileptogenesis. J. Neurosci. Off. J. Soc. Neurosci. *29*, 10979–10988.

Huguet, G., Ey, E., and Bourgeron, T. (2013). The Genetic Landscapes of Autism Spectrum Disorders. Annu. Rev. Genomics Hum. Genet. *14*, 191–213.

Hulbert, S.W., and Jiang, Y.-H. (2016). Monogenic mouse models of autism spectrum disorders: Common mechanisms and missing links. Neuroscience *321*, 3–23.

Ishii, T.M., Takano, M., Xie, L.-H., Noma, A., and Ohmori, H. (1999). Molecular Characterization of the Hyperpolarization-activated Cation Channel in Rabbit Heart Sinoatrial Node. J. Biol. Chem. *274*, 12835–12839.

Ishii, T.M., Takano, M., and Ohmori, H. (2001). Determinants of activation kinetics in mammalian hyperpolarization-activated cation channels. J. Physiol. *537*, 93–100.

Jackson, H.A., Marshall, C.R., and Accili, E.A. (2007). Evolution and structural diversification of hyperpolarization-activated cyclic nucleotide-gated channel genes. Physiol. Genomics *29*, 231–245.

Jamain, S., Quach, H., Betancur, C., Råstam, M., Colineaux, C., Gillberg, I.C., Soderstrom, H., Giros, B., Leboyer, M., Gillberg, C., et al. (2003). Mutations of the X-linked genes encoding neuroligins NLGN3 and NLGN4 are associated with autism. Nat. Genet. *34*, 27–29.

James, P., Halladay, J., and Craig, E.A. (1996). Genomic Libraries and a Host Strain Designed for Highly Efficient Two-Hybrid Selection in Yeast. Genetics *144*, 1425–1436.

Jiang, Y., and Ehlers, M.D. (2013). Modeling Autism by SHANK Gene Mutations in Mice. Neuron *78*, 8–27.

Jiang, Y.-Q., Sun, Q., Tu, H.-Y., and Wan, Y. (2008). Characteristics of HCN channels and their participation in neuropathic pain. Neurochem. Res. *33*, 1979–1989.

Kase, D., and Imoto, K. (2012). The Role of HCN Channels on Membrane Excitability in the Nervous System. J. Signal Transduct. *2012*, e619747.

Kaufmann, W.E., Cortell, R., Kau, A.S.M., Bukelis, I., Tierney, E., Gray, R.M., Cox, C., Capone, G.T., and Stanard, P. (2004). Autism spectrum disorder in fragile X syndrome: Communication, social interaction, and specific behaviors. Am. J. Med. Genet. A. *129A*, 225–234.

Kaupp, U.B., and Seifert, and R. (2001). Molecular Diversity of Pacemaker Ion Channels. Annu. Rev. Physiol. *63*, 235–257.

Kennedy, M.B. (1997). The postsynaptic density at glutamatergic synapses. Trends Neurosci. *20*, 264–268.

Kennedy, M.B. (2000). Signal-processing machines at the postsynaptic density. Science *290*, 750–754.

Kim, J.H., Kim, J.H., Yang, E., Park, J.-H., Yu, Y.S., and Kim, K.-W. (2009). Shank 2 expression coincides with neuronal differentiation in the developing retina. Exp. Mol. Med. *41*, 236–242.

Kleinman, J.M., Ventola, P.E., Pandey, J., Verbalis, A.D., Barton, M., Hodgson, S., Green, J., Dumont-Mathieu, T., Robins, D.L., and Fein, D. (2008). Diagnostic stability in very young children with autism spectrum disorders. J. Autism Dev. Disord. *38*, 606–615.

Kole, M.H., Bräuer, A.U., and Stuart, G.J. (2007). Inherited cortical HCN1 channel loss amplifies dendritic calcium electrogenesis and burst firing in a rat absence epilepsy model. J. Physiol. *578*, 507–525.

Kouser, M., Speed, H.E., Dewey, C.M., Reimers, J.M., Widman, A.J., Gupta, N., Liu, S., Jaramillo, T.C., Bangash, M., Xiao, B., et al. (2013). Loss of predominant Shank3 isoforms results in hippocampus-dependent impairments in behavior and synaptic transmission. J. Neurosci. Off. J. Soc. Neurosci. *33*, 18448–18468.

Kozlowski, A.M., Matson, J.L., Horovitz, M., Worley, J.A., and Neal, D. (2011). Parents' first concerns of their child's development in toddlers with autism spectrum disorders. Dev. Neurorehabilitation *14*, 72–78.

Laumonnier, F., Bonnet-Brilhault, F., Gomot, M., Blanc, R., David, A., Moizard, M.-P., Raynaud, M., Ronce, N., Lemonnier, E., Calvas, P., et al. (2004). X-Linked Mental Retardation and Autism Are Associated with a Mutation in the NLGN4 Gene, a Member of the Neuroligin Family. Am. J. Hum. Genet. *74*, 552–557.

Lee, J., Chung, C., Ha, S., Lee, D., Kim, D.-Y., Kim, H., and Kim, E. (2015). Shank3-mutant mice lacking exon 9 show altered excitation/inhibition balance, enhanced rearing, and spatial memory deficit. Front. Cell. Neurosci. *9*.

Leresche, N., Jassik-Gerschenfeld, D., Haby, M., Soltesz, I., and Crunelli, V. (1990). Pacemaker-like and other types of spontaneous membrane potential oscillations of thalamocortical cells. Neurosci. Lett. *113*, 72–77.

Leresche, N., Lightowler, S., Soltesz, I., Jassik-Gerschenfeld, D., and Crunelli, V. (1991). Low-frequency oscillatory activities intrinsic to rat and cat thalamocortical cells. J. Physiol. *441*, 155–174.

Levy, S.E., Giarelli, E., Lee, L.-C., Schieve, L.A., Kirby, R.S., Cunniff, C., Nicholas, J., Reaven, J., and Rice, C.E. (2010). Autism spectrum disorder and co-occurring developmental, psychiatric, and medical conditions among children in multiple populations of the United States. J. Dev. Behav. Pediatr. JDBP *31*, 267–275.

Lim, S., Naisbitt, S., Yoon, J., Hwang, J.I., Suh, P.G., Sheng, M., and Kim, E. (1999). Characterization of the Shank family of synaptic proteins. Multiple genes, alternative splicing, and differential expression in brain and development. J. Biol. Chem. *274*, 29510–29518.

Lim, S., Sala, C., Yoon, J., Park, S., Kuroda, S., Sheng, M., and Kim, E. (2001). Sharpin, a novel postsynaptic density protein that directly interacts with the shank family of proteins. Mol. Cell. Neurosci. *17*, 385–397.

Lord, C., Risi, S., DiLavore, P.S., Shulman, C., Thurm, A., and Pickles, A. (2006). Autism from 2 to 9 years of age. Arch. Gen. Psychiatry *63*, 694–701.

Lörincz, A., Notomi, T., Tamás, G., Shigemoto, R., and Nusser, Z. (2002). Polarized and compartment-dependent distribution of HCN1 in pyramidal cell dendrites. Nat. Neurosci. *5*, 1185–1193.

Ludwig, A., Zong, X., Jeglitsch, M., Hofmann, F., and Biel, M. (1998). A family of hyperpolarization-activated mammalian cation channels. Nature *393*, 587–591.

Ludwig, A., Zong, X., Stieber, J., Hullin, R., Hofmann, F., and Biel, M. (1999). Two pacemaker channels from human heart with profoundly different activation kinetics. EMBO J. *18*, 2323–2329.

Ludwig, A., Budde, T., Stieber, J., Moosmang, S., Wahl, C., Holthoff, K., Langebartels, A., Wotjak, C., Munsch, T., Zong, X., et al. (2003). Absence epilepsy and sinus dysrhythmia in mice lacking the pacemaker channel HCN2. EMBO J. *22*, 216–224.

Lupica, C.R., Bell, J.A., Hoffman, A.F., and Watson, P.L. (2001). Contribution of the hyperpolarization-activated current (I(h)) to membrane potential and GABA release in hippocampal interneurons. J. Neurophysiol. *86*, 261–268.

MacGillavry, H.D., Kerr, J.M., Kassner, J., Frost, N.A., and Blanpied, T.A. (2016). Shank–cortactin interactions control actin dynamics to maintain flexibility of neuronal spines and synapses. Eur. J. Neurosci. *43*, 179–193.

Macri, V., and Accili, E.A. (2004). Structural Elements of Instantaneous and Slow Gating in Hyperpolarization-activated Cyclic Nucleotide-gated Channels. J. Biol. Chem. *279*, 16832–16846.

Magee, J.C. (1998). Dendritic hyperpolarization-activated currents modify the integrative properties of hippocampal CA1 pyramidal neurons. J. Neurosci. Off. J. Soc. Neurosci. *18*, 7613–7624.

Magee, J.C. (1999). Dendritic Ih normalizes temporal summation in hippocampal CA1 neurons. Nat. Neurosci. *2*, 848–848.

Magee, J.C. (2000). Dendritic integration of excitatory synaptic input. Nat. Rev. Neurosci. *1*, 181–190.

Mameza, M.G., Dvoretskova, E., Bamann, M., Hönck, H.-H., Güler, T., Boeckers, T.M., Schoen, M., Verpelli, C., Sala, C., Barsukov, I., et al. (2013). SHANK3 Gene Mutations Associated with Autism Facilitate Ligand Binding to the Shank3 Ankyrin Repeat Region. J. Biol. Chem. *288*, 26697–26708.

Marshall, C.R., Noor, A., Vincent, J.B., Lionel, A.C., Feuk, L., Skaug, J., Shago, M., Moessner, R., Pinto, D., Ren, Y., et al. (2008). Structural Variation of Chromosomes in Autism Spectrum Disorder. Am. J. Hum. Genet. *82*, 477–488.

Mayer, M.L., and Westbrook, G.L. (1983). A voltage-clamp analysis of inward (anomalous) rectification in mouse spinal sensory ganglion neurones. J. Physiol. *340*, 19–45.

McCormick, D.A., and Pape, H.C. (1990). Properties of a hyperpolarization-activated cation current and its role in rhythmic oscillation in thalamic relay neurones. J. Physiol. *431*, 291–318.

Mei, Y., Monteiro, P., Zhou, Y., Kim, J.-A., Gao, X., Fu, Z., and Feng, G. (2016). Adult restoration of Shank3 expression rescues selective autistic-like phenotypes. Nature *530*, 481–484.

Meuth, S.G., Kanyshkova, T., Meuth, P., Landgraf, P., Munsch, T., Ludwig, A., Hofmann, F., Pape, H.-C., and Budde, T. (2006). Membrane resting potential of thalamocortical relay neurons is shaped by the interaction among TASK3 and HCN2 channels. J. Neurophysiol. *96*, 1517–1529.

Meyer, D., Bonhoeffer, T., and Scheuss, V. (2014). Balance and stability of synaptic structures during synaptic plasticity. Neuron *82*, 430–443.

Milligan, C.J., Edwards, I.J., and Deuchars, J. (2006). HCN1 ion channel immunoreactivity in spinal cord and medulla oblongata. Brain Res. *1081*, 79–91.

Moessner, R., Marshall, C.R., Sutcliffe, J.S., Skaug, J., Pinto, D., Vincent, J., Zwaigenbaum, L., Fernandez, B., Roberts, W., Szatmari, P., et al. (2007). Contribution of SHANK3 mutations to autism spectrum disorder. Am. J. Hum. Genet. *81*, 1289–1297.

Momin, A., Cadiou, H., Mason, A., and McNaughton, P.A. (2008). Role of the hyperpolarization-activated current Ih in somatosensory neurons. J. Physiol. *586*, 5911–5929.

Monteggia, L.M., Eisch, A.J., Tang, M.D., Kaczmarek, L.K., and Nestler, E.J. (2000). Cloning and localization of the hyperpolarization-activated cyclic nucleotide-gated channel family in rat brain. Mol. Brain Res. *81*, 129–139.

Monteiro, P., and Feng, G. (2017). SHANK proteins: roles at the synapse and in autism spectrum disorder. Nat. Rev. Neurosci. *18*, 147–157.

Moosmang, S., Biel, M., Hofmann, F., and Ludwig, A. (1999). Differential distribution of four hyperpolarization-activated cation channels in mouse brain. Biol. Chem. *380*, 975–980.

Moosmang, S., Stieber, J., Zong, X., Biel, M., Hofmann, F., and Ludwig, A. (2001). Cellular expression and functional characterization of four hyperpolarization-activated pacemaker channels in cardiac and neuronal tissues. Eur. J. Biochem. *268*, 1646–1652.

Moroni, A., Barbuti, A., Altomare, C., Viscomi, C., Morgan, J., Baruscotti, M., and DiFrancesco, D. (2000). Kinetic and ionic properties of the human HCN2 pacemaker channel. Pflugers Arch. *439*, 618–626.

Naisbitt, S., Kim, E., Tu, J.C., Xiao, B., Sala, C., Valtschanoff, J., Weinberg, R.J., Worley, P.F., and Sheng, M. (1999). Shank, a Novel Family of Postsynaptic Density Proteins that Binds to the NMDA Receptor/PSD-95/GKAP Complex and Cortactin. Neuron *23*, 569–582.

Nakamura, Y., Shi, X., Numata, T., Mori, Y., Inoue, R., Lossin, C., Baram, T.Z., and Hirose, S. (2013). Novel HCN2 Mutation Contributes to Febrile Seizures by Shifting the Channel's Kinetics in a Temperature-Dependent Manner. PLOS ONE *8*, e80376.

Nava, C., Dalle, C., Rastetter, A., Striano, P., de Kovel, C.G.F., Nabbout, R., Cancès, C., Ville, D., Brilstra, E.H., Gobbi, G., et al. (2014). De novo mutations in HCN1 cause early infantile epileptic encephalopathy. Nat. Genet. *46*, 640–645.

Nolan, M.F., Dudman, J.T., Dodson, P.D., and Santoro, B. (2007). HCN1 Channels Control Resting and Active Integrative Properties of Stellate Cells from Layer II of the Entorhinal Cortex. J. Neurosci. *27*, 12440–12451.

Noma, A., and Irisawa, H. (1976). Membrane currents in the rabbit sinoatrial node cell as studied by the double microelectrode method. Pflüg. Arch. *364*, 45–52.

Notomi, T., and Shigemoto, R. (2004). Immunohistochemical localization of Ih channel subunits, HCN1-4, in the rat brain. J. Comp. Neurol. *471*, 241–276.

O'Roak, B.J., Deriziotis, P., Lee, C., Vives, L., Schwartz, J.J., Girirajan, S., Karakoc, E., MacKenzie, A.P., Ng, S.B., Baker, C., et al. (2011). Exome sequencing in sporadic autism spectrum disorders identifies severe de novo mutations. Nat. Genet. *43*, 585–589.

Ozonoff, S., Young, G.S., Carter, A., Messinger, D., Yirmiya, N., Zwaigenbaum, L., Bryson, S., Carver, L.J., Constantino, J.N., Dobkins, K., et al. (2011). Recurrence Risk for Autism Spectrum Disorders: A Baby Siblings Research Consortium Study. Pediatrics peds.2010-2825.

Pape, H.C. (1996). Queer current and pacemaker: the hyperpolarization-activated cation current in neurons. Annu. Rev. Physiol. *58*, 299–327.

Park, E., Na, M., Choi, J., Kim, S., Lee, J.-R., Yoon, J., Park, D., Sheng, M., and Kim, E. (2003). The Shank family of postsynaptic density proteins interacts with and promotes synaptic accumulation of the beta PIX guanine nucleotide exchange factor for Rac1 and Cdc42. J. Biol. Chem. *278*, 19220–19229.

Peça, J., Feliciano, C., Ting, J.T., Wang, W., Wells, M.F., Venkatraman, T.N., Lascola, C.D., Fu, Z., and Feng, G. (2011). Shank3 mutant mice display autistic-like behaviours and striatal dysfunction. Nature *472*, 437–442.

Phelan, K., and McDermid, H.E. (2012). The 22q13.3 Deletion Syndrome (Phelan-McDermid Syndrome). Mol. Syndromol. *2*, 186–201.

Phillips, A.M., Kim, T., Vargas, E., Petrou, S., and Reid, C.A. (2014). Spike-and-wave discharge mediated reduction in hippocampal HCN1 channel function associates with learning deficits in a genetic mouse model of epilepsy. Neurobiol. Dis. *64*, 30–35.

Poolos, N.P. (2012). Hyperpolarization-Activated Cyclic Nucleotide-Gated (HCN) Ion Channelopathy in Epilepsy. In Jasper's Basic Mechanisms of the Epilepsies, J.L. Noebels, M. Avoli, M.A. Rogawski, R.W. Olsen, and A.V. Delgado-Escueta, eds. (Bethesda (MD): National Center for Biotechnology Information (US)), p.

Poolos, N.P., Migliore, M., and Johnston, D. (2002). Pharmacological upregulation of h-channels reduces the excitability of pyramidal neuron dendrites. Nat. Neurosci. *5*, 767–774.

Poolos, N.P., Bullis, J.B., and Roth, M.K. (2006). Modulation of h-channels in hippocampal pyramidal neurons by p38 mitogen-activated protein kinase. J. Neurosci. Off. J. Soc. Neurosci. *26*, 7995–8003.

Proenza, C., Angoli, D., Agranovich, E., Macri, V., and Accili, E.A. (2002). Pacemaker Channels Produce an Instantaneous Current. J. Biol. Chem. *277*, 5101–5109.

Qualmann, B., Boeckers, T.M., Jeromin, M., Gundelfinger, E.D., and Kessels, M.M. (2004). Linkage of the actin cytoskeleton to the postsynaptic density via direct interactions of Abp1 with the ProSAP/Shank family. J. Neurosci. Off. J. Soc. Neurosci. *24*, 2481–2495.

Raynaud, F., Janossy, A., Dahl, J., Bertaso, F., Perroy, J., Varrault, A., Vidal, M., Worley, P.F., Boeckers, T.M., Bockaert, J., et al. (2013). Shank3-Rich2 interaction regulates AMPA receptor recycling and synaptic long-term potentiation. J. Neurosci. Off. J. Soc. Neurosci. *33*, 9699–9715.

Robinson, R.B., and Siegelbaum, S.A. (2003). Hyperpolarization-activated cation currents: from molecules to physiological function. Annu. Rev. Physiol. *65*, 453–480.

Rogawski, M.A. (2013). AMPA receptors as a molecular target in epilepsy therapy. Acta Neurol. Scand. Suppl. 9–18.

Rosenberg, R.E., Law, J.K., Yenokyan, G., McGready, J., Kaufmann, W.E., and Law, P.A. (2009). Characteristics and concordance of autism spectrum disorders among 277 twin pairs. Arch. Pediatr. Adolesc. Med. *163*, 907–914.

Roussignol, G., Ango, F., Romorini, S., Tu, J.C., Sala, C., Worley, P.F., Bockaert, J., and Fagni, L. (2005). Shank expression is sufficient to induce functional dendritic spine synapses in aspiny neurons. J. Neurosci. Off. J. Soc. Neurosci. *25*, 3560–3570.

Sala, C., Piëch, V., Wilson, N.R., Passafaro, M., Liu, G., and Sheng, M. (2001). Regulation of dendritic spine morphology and synaptic function by Shank and Homer. Neuron *31*, 115–130.

Santoro, B., Grant, S.G.N., Bartsch, D., and Kandel, E.R. (1997). Interactive cloning with the SH3 domain of N-src identifies a new brain specific ion channel protein, with homology to Eag and cyclic nucleotide-gated channels. Proc. Natl. Acad. Sci. U. S. A. *94*, 14815–14820.

Santoro, B., Liu, D.T., Yao, H., Bartsch, D., Kandel, E.R., Siegelbaum, S.A., and Tibbs, G.R. (1998). Identification of a gene encoding a hyperpolarization-activated pacemaker channel of brain. Cell *93*, 717–729.

Santoro, B., Chen, S., Luthi, A., Pavlidis, P., Shumyatsky, G.P., Tibbs, G.R., and Siegelbaum, S.A. (2000). Molecular and functional heterogeneity of hyperpolarization-activated pacemaker channels in the mouse CNS. J. Neurosci. Off. J. Soc. Neurosci. *20*, 5264–5275.

Sarowar, T., and Grabrucker, A.M. (2016). Actin-Dependent Alterations of Dendritic Spine Morphology in Shankopathies. Neural Plast. *2016*.

Schendel, D., and Bhasin, T.K. (2008). Birth weight and gestational age characteristics of children with autism, including a comparison with other developmental disabilities. Pediatrics *121*, 1155–1164.

Schmeisser, M.J., Ey, E., Wegener, S., Bockmann, J., Stempel, A.V., Kuebler, A., Janssen, A.-L., Udvardi, P.T., Shiban, E., Spilker, C., et al. (2012). Autistic-like behaviours and hyperactivity in mice lacking ProSAP1/Shank2. Nature *486*, 256–260.

Sebat, J., Lakshmi, B., Malhotra, D., Troge, J., Lese-Martin, C., Walsh, T., Yamrom, B., Yoon, S., Krasnitz, A., Kendall, J., et al. (2007). Strong Association of De Novo Copy Number Mutations with Autism. Science *316*, 445–449.

Seifert, R., Scholten, A., Gauss, R., Mincheva, A., Lichter, P., and Kaupp, U.B. (1999). Molecular characterization of a slowly gating human hyperpolarization-activated channel predominantly expressed in thalamus, heart, and testis. Proc. Natl. Acad. Sci. U. S. A. *96*, 9391–9396.

Seoh, S.-A., Sigg, D., Papazian, D.M., and Bezanilla, F. (1996). Voltage-Sensing Residues in the S2 and S4 Segments of the Shaker K+ Channel. Neuron *16*, 1159–1167.

Sheng, M., and Hoogenraad, C.C. (2007). The postsynaptic architecture of excitatory synapses: a more quantitative view. Annu. Rev. Biochem. *76*, 823–847.

Sheng, M., and Kim, E. (2000). The Shank family of scaffold proteins. J. Cell Sci. *113 (Pt 11)*, 1851–1856.

Sheng, M., and Kim, M.J. (2002). Postsynaptic signaling and plasticity mechanisms. Science *298*, 776–780.

Shipton, O.A., and Paulsen, O. (2014). GluN2A and GluN2B subunit-containing NMDA receptors in hippocampal plasticity. Philos. Trans. R. Soc. B Biol. Sci. *369*.

Simonoff, E., Pickles, A., Charman, T., Chandler, S., Loucas, T., and Baird, G. (2008). Psychiatric Disorders in Children With Autism Spectrum Disorders: Prevalence, Comorbidity, and Associated Factors in a Population-Derived Sample. J. Am. Acad. Child Adolesc. Psychiatry *47*, 921–929.

Smalley, S.L. (1998). Autism and Tuberous Sclerosis. J. Autism Dev. Disord. *28*, 407–414.

Solomon, J.S., and Nerbonne, J.M. (1993). Hyperpolarization-activated currents in isolated superior colliculus-projecting neurons from rat visual cortex. J. Physiol. *462*, 393–420.

Song, I., and Huganir, R.L. (2002). Regulation of AMPA receptors during synaptic plasticity. Trends Neurosci. *25*, 578–588.

Speed, H.E., Kouser, M., Xuan, Z., Reimers, J.M., Ochoa, C.F., Gupta, N., Liu, S., and Powell, C.M. (2015). Autism-Associated Insertion Mutation (InsG) of Shank3 Exon 21 Causes Impaired Synaptic Transmission and Behavioral Deficits. J. Neurosci. *35*, 9648–9665.

Stieber, J., Stöckl, G., Herrmann, S., Hassfurth, B., and Hofmann, F. (2005). Functional Expression of the Human HCN3 Channel. J. Biol. Chem. *280*, 34635–34643.

Stuart, G.J., and Spruston, N. (2015). Dendritic integration: 60 years of progress. Nat. Neurosci. *18*, 1713–1721.

Sumi, S., Taniai, H., Miyachi, T., and Tanemura, M. (2006). Sibling risk of pervasive developmental disorder estimated by means of an epidemiologic survey in Nagoya, Japan. J. Hum. Genet. *51*, 518–522.

Tang, B., Sander, T., Craven, K.B., Hempelmann, A., and Escayg, A. (2008). Mutation analysis of the hyperpolarization-activated cyclic nucleotide-gated channels HCN1 and HCN2 in idiopathic generalized epilepsy. Neurobiol. Dis. *29*, 59–70.

Taniai, H., Nishiyama, T., Miyachi, T., Imaeda, M., and Sumi, S. (2008). Genetic influences on the broad spectrum of autism: study of proband-ascertained twins. Am. J. Med. Genet. Part B Neuropsychiatr. Genet. Off. Publ. Int. Soc. Psychiatr. Genet. *147B*, 844–849.

Tu, J.C., Xiao, B., Naisbitt, S., Yuan, J.P., Petralia, R.S., Brakeman, P., Doan, A., Aakalu, V.K., Lanahan, A.A., Sheng, M., et al. (1999). Coupling of mGluR/Homer and PSD-95 Complexes by the Shank Family of Postsynaptic Density Proteins. Neuron *23*, 583–592.

Uchino, S., Wada, H., Honda, S., Nakamura, Y., Ondo, Y., Uchiyama, T., Tsutsumi, M., Suzuki, E., Hirasawa, T., and Kohsaka, S. (2006). Direct interaction of post-synaptic density-95/Dlg/ZO-1 domain-containing synaptic molecule Shank3 with GluR1 α-amino-3-hydroxy-5-methyl-4-isoxazole propionic acid receptor. J. Neurochem. *97*, 1203–1214.

Uruno, T., Liu, J., Zhang, P., Fan Yx, null, Egile, C., Li, R., Mueller, S.C., and Zhan, X. (2001). Activation of Arp2/3 complex-mediated actin polymerization by cortactin. Nat. Cell Biol. *3*, 259–266.

Vaca, L., Stieber, J., Zong, X., Ludwig, A., Hofmann, F., and Biel, M. (2000). Mutations in the S4 domain of a pacemaker channel alter its voltage dependence. FEBS Lett. *479*, 35–40.

Van Criekinge, W., and Beyaert, R. (1999). Yeast Two-Hybrid: State of the Art. Biol. Proced. Online *2*, 1–38.

Verpelli, C., Dvoretskova, E., Vicidomini, C., Rossi, F., Chiappalone, M., Schoen, M., Di Stefano, B., Mantegazza, R., Broccoli, V., Böckers, T.M., et al. (2011). Importance of Shank3 protein in regulating metabotropic glutamate receptor 5 (mGluR5) expression and signaling at synapses. J. Biol. Chem. *286*, 34839–34850.

Vijayraghavan, S., Wang, M., Birnbaum, S.G., Williams, G.V., and Arnsten, A.F.T. (2007). Inverted-U dopamine D1 receptor actions on prefrontal neurons engaged in working memory. Nat. Neurosci. *10*, 376–384.

Virkud, Y.V., Todd, R.D., Abbacchi, A.M., Zhang, Y., and Constantino, J.N. (2009). Familial Aggregation of Quantitative Autistic Traits in Multiplex versus Simplex Autism. Am. J. Med. Genet. Part B Neuropsychiatr. Genet. Off. Publ. Int. Soc. Psychiatr. Genet. *150B*, 328–334.

Viscomi, C., Altomare, C., Bucchi, A., Camatini, E., Baruscotti, M., Moroni, A., and DiFrancesco, D. (2001). C terminus-mediated control of voltage and cAMP gating of hyperpolarization-activated cyclic nucleotide-gated channels. J. Biol. Chem. *276*, 29930–29934.

Waga, C., Asano, H., Sanagi, T., Suzuki, E., Nakamura, Y., Tsuchiya, A., Itoh, M., Goto, Y., Kohsaka, S., and Uchino, S. (2014). Identification of two novel Shank3 transcripts in the developing mouse neocortex. J. Neurochem. *128*, 280–293.

Wainger, B.J., DeGennaro, M., Santoro, B., Siegelbaum, S.A., and Tibbs, G.R. (2001). Molecular mechanism of cAMP modulation of HCN pacemaker channels. Nature *411*, 805–810.

Wang, J., Chen, S., and Siegelbaum, S.A. (2001). Regulation of hyperpolarization-activated HCN channel gating and cAMP modulation due to interactions of COOH terminus and core transmembrane regions. J. Gen. Physiol. *118*, 237–250.

Wang, M., Ramos, B.P., Paspalas, C.D., Shu, Y., Simen, A., Duque, A., Vijayraghavan, S., Brennan, A., Dudley, A., Nou, E., et al. (2007). α2A-Adrenoceptors Strengthen Working Memory Networks by Inhibiting cAMP-HCN Channel Signaling in Prefrontal Cortex. Cell *129*, 397–410.

Wang, M., Gamo, N.J., Yang, Y., Jin, L.E., Wang, X.-J., Laubach, M., Mazer, J.A., Lee, D., and Arnsten, A.F.T. (2011a). Neuronal basis of age-related working memory decline. Nature *476*, 210–213.

Wang, X., McCoy, P.A., Rodriguiz, R.M., Pan, Y., Je, H.S., Roberts, A.C., Kim, C.J., Berrios, J., Colvin, J.S., Bousquet-Moore, D., et al. (2011b). Synaptic dysfunction and abnormal behaviors in mice lacking major isoforms of Shank3. Hum. Mol. Genet. *20*, 3093–3108.

Wang, X., Xu, Q., Bey, A.L., Lee, Y., and Jiang, Y. (2014a). Transcriptional and functional complexity of Shank3 provides a molecular framework to understand the phenotypic heterogeneity of SHANK3 causing autism and Shank3 mutant mice. Mol. Autism *5*, 30.

Wang, X., Bey, A.L., Chung, L., Krystal, A.D., and Jiang, Y.-H. (2014b). Therapeutic approaches for shankopathies. Dev. Neurobiol. *74*, 123–135.

Wang, X., Bey, A.L., Katz, B.M., Badea, A., Kim, N., David, L.K., Duffney, L.J., Kumar, S., Mague, S.D., Hulbert, S.W., et al. (2016). Altered mGluR5-Homer scaffolds and corticostriatal connectivity in a *Shank3* complete knockout model of autism. Nat. Commun. *7*, ncomms11459.

Weaver, A.M., Karginov, A.V., Kinley, A.W., Weed, S.A., Li, Y., Parsons, J.T., and Cooper, J.A. (2001). Cortactin promotes and stabilizes Arp2/3-induced actin filament network formation. Curr. Biol. CB *11*, 370–374.

Wendholt, D., Spilker, C., Schmitt, A., Dolnik, A., Smalla, K.-H., Proepper, C., Bockmann, J., Sobue, K., Gundelfinger, E.D., Kreutz, M.R., et al. (2006). ProSAP-interacting Protein 1 (ProSAPiP1), a Novel Protein of the Postsynaptic Density That Links the Spine-associated Rap-Gap (SPAR) to the Scaffolding Protein ProSAP2/Shank3. J. Biol. Chem. *281*, 13805–13816.

Whitaker, G.M., Angoli, D., Nazzari, H., Shigemoto, R., and Accili, E.A. (2007). HCN2 and HCN4 Isoforms Self-assemble and Co-assemble with Equal Preference to Form Functional Pacemaker Channels. J. Biol. Chem. *282*, 22900–22909.

Williams, S.R., and Stuart, G.J. (2000). Site independence of EPSP time course is mediated by dendritic I(h) in neocortical pyramidal neurons. J. Neurophysiol. *83*, 3177–3182.

Ye, B., and Nerbonne, J.M. (2009). Proteolytic Processing of HCN2 and Co-assembly with HCN4 in the Generation of Cardiac Pacemaker Channels. J. Biol. Chem. *284*, 25553–25559.

Yi, F., Danko, T., Botelho, S.C., Patzke, C., Pak, C., Wernig, M., and Südhof, T.C. (2016). Autism-associated SHANK3 haploinsufficiency causes Ih channelopathy in human neurons. Science aaf2669.

Yu, F.H., and Catterall, W.A. (2004). The VGL-chanome: a protein superfamily specialized for electrical signaling and ionic homeostasis. Sci. STKE Signal Transduct. Knowl. Environ. *2004*, re15.

Yu, F.H., Yarov-Yarovoy, V., Gutman, G.A., and Catterall, W.A. (2005). Overview of Molecular Relationships in the Voltage-Gated Ion Channel Superfamily. Pharmacol. Rev. *57*, 387–395.

Zagotta, W.N., Olivier, N.B., Black, K.D., Young, E.C., Olson, R., and Gouaux, E. (2003). Structural basis for modulation and agonist specificity of HCN pacemaker channels. Nature *425*, 200–205.

Zatkova, M., Bakos, J., Hodosy, J., and Ostatnikova, D. (2016). Synapse alterations in autism: Review of animal model findings. Biomed. Pap. Med. Fac. Univ. Palacky Olomouc Czechoslov. *160*, 201–210.

Zecavati, N., and Spence, S.J. (2009). Neurometabolic disorders and dysfunction in autism spectrum disorders. Curr. Neurol. Neurosci. Rep. *9*, 129–136.

Zhang, Q., Huang, A., Lin, Y.-C., and Yu, H.-G. (2009). Associated changes in HCN2 and HCN4 transcripts and If pacemaker current in myocytes. Biochim. Biophys. Acta BBA - Biomembr. *1788*, 1138–1147.

Zhou, Y., Kaiser, T., Monteiro, P., Zhang, X., Van der Goes, M.S., Wang, D., Barak, B., Zeng, M., Li, C., Lu, C., et al. (2016). Mice with Shank3 Mutations Associated with ASD and Schizophrenia Display Both Shared and Distinct Defects. Neuron *89*, 147–162.

Zhu, L., Wang, X., Li, X.-L., Towers, A., Cao, X., Wang, P., Bowman, R., Yang, H., Goldstein, J., Li, Y.-J., et al. (2014). Epigenetic dysregulation of SHANK3 in brain tissues from individuals with autism spectrum disorders. Hum. Mol. Genet. *23*, 1563–1578.

Ziff, E.B. (1997). Enlightening the postsynaptic density. Neuron *19*, 1163–1174.

Zoghbi, H.Y. (2003). Postnatal neurodevelopmental disorders: meeting at the synapse? Science *302*, 826–830.

APPENDICES

A

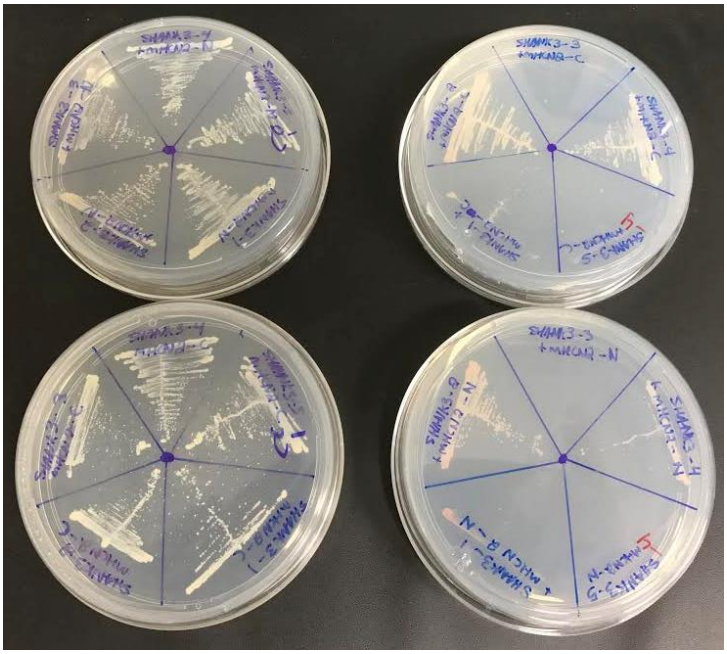

B

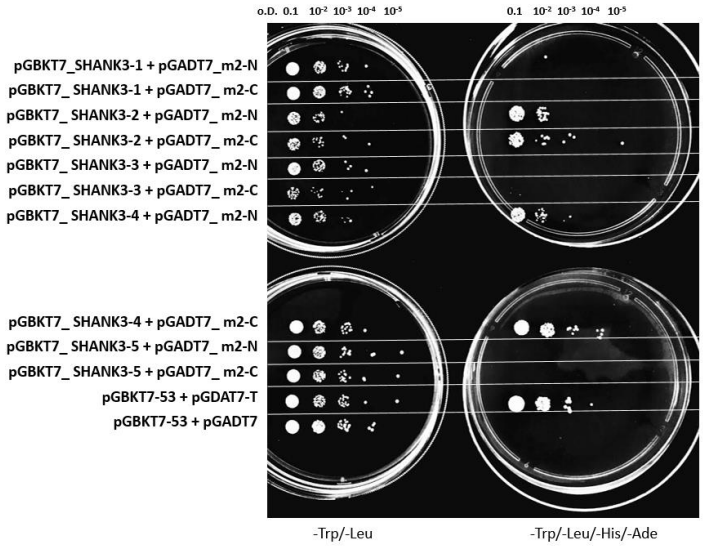

Supplementary Figure 1. The yeast two-hybrid assay of pGBKT7_SHANK3 bait plasmids with pGADT7_m1 & m2 prey plasmids. A. Top left: control plate (-Leu/-Trp) selecting for successful co-transformation of pGBKT7_SHANK3-1, pGBKT7_SHANK3-2, pGBKT7_SHANK3-3, pGBKT7_SHANK3-4, and pGBKT7_SHANK3-5 with pGADT7_m1-N. Bottom left: control plate (-Leu/-Trp) selecting for successful co-transformation of pGBKT7_SHANK3-1, pGBKT7_SHANK3-2, pGBKT7_SHANK3-3, pGBKT7_SHANK3-4, and pGBKT7_SHANK3-5 with pGADT7_m2-N. Top right: assay plate (-Leu/-Trp/-His/-Ade) selecting for interactions between pGBKT7_SHANK3-1, pGBKT7_SHANK3-2, pGBKT7_SHANK3-3, pGBKT7_SHANK3-4, and pGBKT7_SHANK3-5 with pGADT7_m1-N. Bottom right: assay plate (-Leu/-Trp/-His/-Ade) selecting for interactions between pGBKT7_SHANK3-1, pGBKT7_SHANK3-2, pGBKT7_SHANK3-3, pGBKT7_SHANK3-4, and pGBKT7_SHANK3-5 with pGADT7_m2-N. B. pGBKT7_SHANK3-1, pGBKT7_SHANK3-2, pGBKT7_SHANK3-3, pGBKT7_SHANK3-4, and pGBKT7_SHANK3-5 were each co-transformed with pGADT7_m2-N and pGADT7_m2-C; m1-CNBD plasmids into AH109 and grown on depleted Trp-/Leu-SD agar plates. Individual colonies were selected and grown in depleted Trp-/Leu-SD media until the optical density (o.D.) of each sample was measure to 0.1. Samples were serial diluted to 10^{-1}, 10^{-2}, 10^{-3}, 10^{-4} and, 10^{-5} and then plated onto Trp-/Leu-(left) and Trp-/Leu-/His-/Ade-(right) agar plates as seen above.

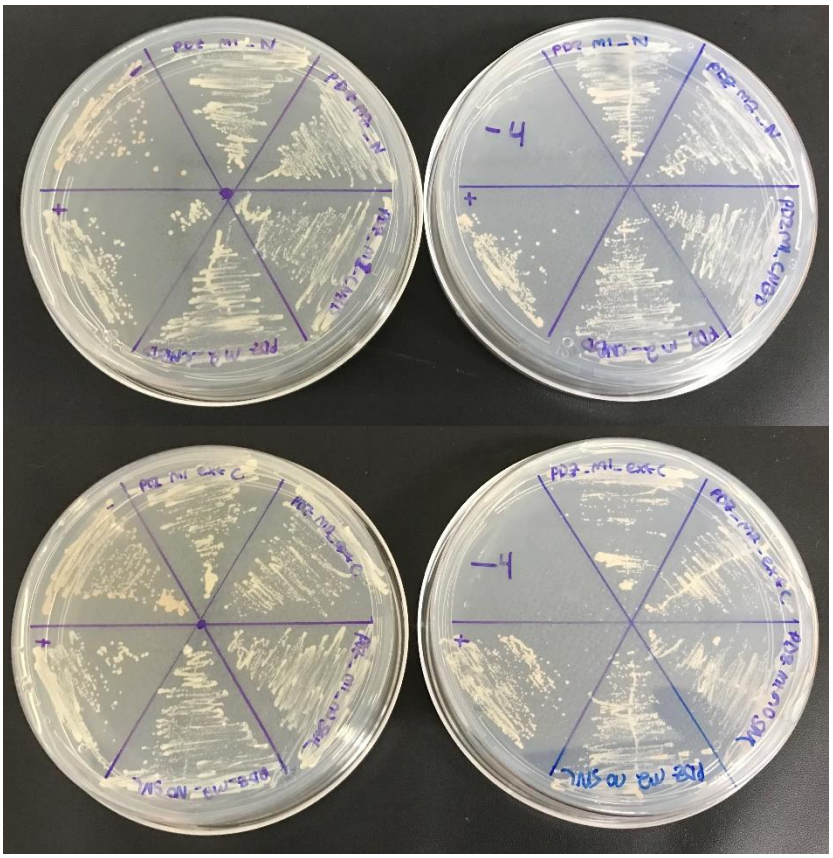

Supplementary Figure 2. The yeast two-hybrid assay of pGBKT7_SHANK3_PDZ bait plasmids with pGADT7_m1 & m2 prey plasmids. A. Top left: control plate (-Leu/-Trp) selecting for successful co-transformation of pGBKT7_SHANK3_PDZ with pGADT7_m1-N, pGADT7_m1-CNBD, pGADT7_m1-ext-C, and pGADT7_m1-ext-C-noSNL. Bottom left: control plate (-Leu/-Trp) selecting for successful co-transformation of pGBKT7_SHANK3_PDZ with pGADT7_m2-N, pGADT7_m2-CNBD, pGADT7_m2-ext-C, and pGADT7_m2-ext-C-noSNL. Top right: assay plate (-Leu/-Trp/-His/-Ade) selecting for interactions between pGBKT7_SHANK3_PDZ with pGADT7_m1-N, pGADT7_m1-CNBD, pGADT7_m1-ext-C, and pGADT7_m1-ext-C-noSNL. Bottom right: assay plate (-Leu/-Trp/-His/-Ade) selecting for interactions of pGBKT7_SHANK3_PDZ with pGADT7_m2-N, pGADT7_m2-CNBD, pGADT7_m2-ext-C, and pGADT7_m2-ext-C-noSNL.

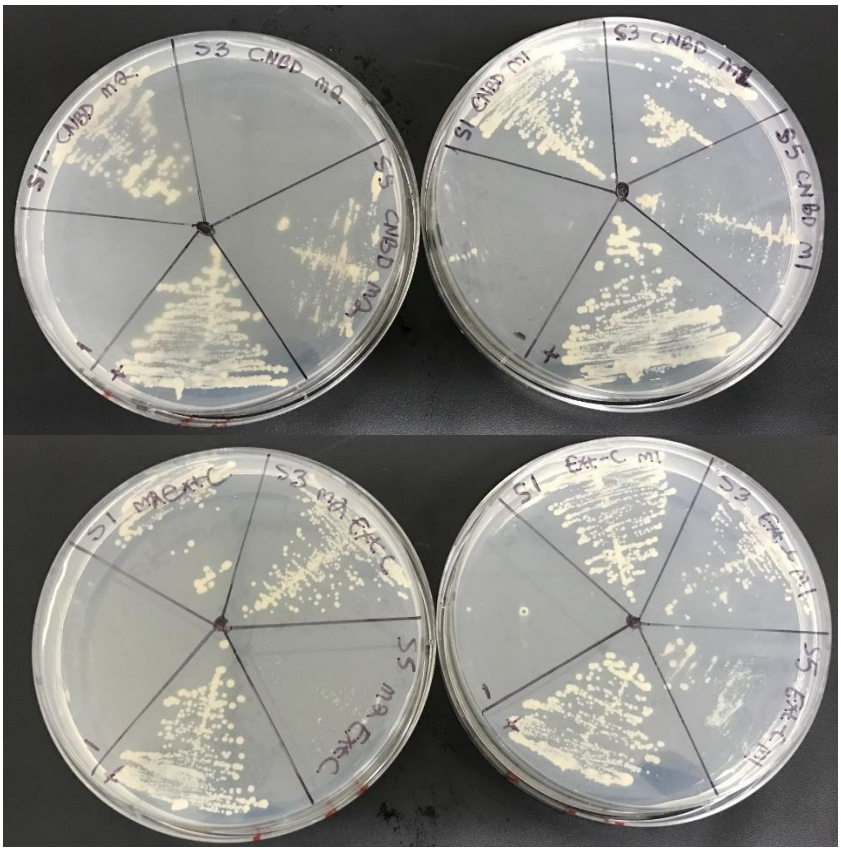

Supplementary Figure 3. The yeast two-hybrid assay of pGBKT7_SHANK3-1, pGBKT7_SHANK3-3, and pGBKT7_SHANK3-5 bait plasmids with the pGADT7_m1-CNBD, pGADT7_m2-CNBD, pGADT7_m1-ext-C, and pGADT7_m2-ext-C prey plasmids. Top left: assay plate (-Leu/-Trp/-His/) selecting for interactions between pGBKT7_SHANK3-1, pGBKT7_SHANK3-3, and pGBKT7_SHANK3-5 bait plasmids with pGADT7_m2-CNBD. Bottom left: assay plate (-Leu/-Trp/-His/) selecting for interactions between pGBKT7_SHANK3-1, pGBKT7_SHANK3-3, and pGBKT7_SHANK3-5 bait plasmids with pGADT7_m2-ext-C. Top right: assay plate (-Leu/-Trp/-His/) selecting for interactions between pGBKT7_SHANK3-1, pGBKT7_SHANK3-3, and pGBKT7_SHANK3-5 bait plasmids with pGADT7_m1-CNBD. Bottom right: assay plate (-Leu/-Trp/-His/) selecting for interactions between pGBKT7_SHANK3-1, pGBKT7_SHANK3-3, and pGBKT7_SHANK3-5 bait plasmids with pGADT7_m1-ext-C.

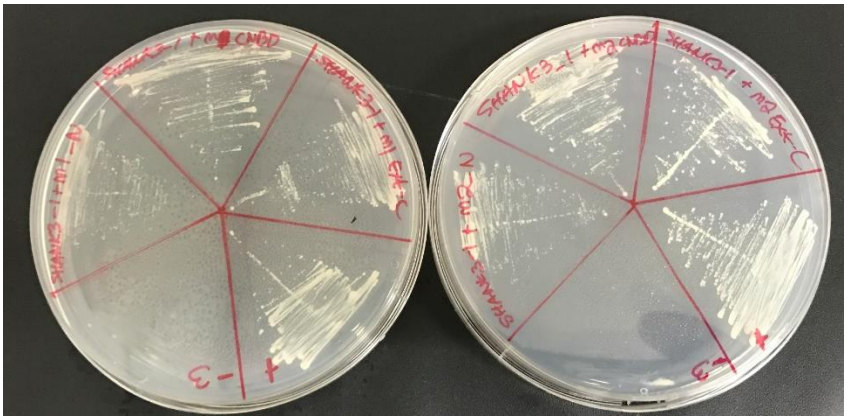

Supplementary Figure 4. The yeast two-hybrid assay of pGBKT7_SHANK3-1 bait plasmid with pGADT7_m1-N, pGADT7_m2-N, pGADT7_m1-CNBD, pGADT7_m2-CNBD, pGADT7_m1-ext-C, pGADT7_m2-ext-C. Left: assay plate (-Leu/-Trp/-His/) selecting for interactions between pGBKT7_SHANK3-1 and pGADT7_m1-N, pGADT7_m1-CNBD, and pGADT7_m1-ext-C. Right: assay plate (-Leu/-Trp/-His/) selecting for interactions between pGBKT7_SHANK3-1 and pGADT7_m2-N, pGADT7_m2-CNBD, and pGADT7_m2-ext-C.

Vita

Nikhil N. Shah was born on May 9th, 1988 in Salem, Virginia. He graduate from Glenvar High School in June, 2006. He received his Bachelor of Science from Virginia Polytechnic Institute and State University in August, 2012 and went on to receive a Master of Science in Physiology and Biophysics from Virginia Commonwealth University in August, 2017. He is now an M.D. candidate at the Virginia Commonwealth University School of Medicine for the Class of 2021.